ACS APPLIED POLYMER MATERIALS

pubs.acs.org/acsapm

Article

Meso-π-Extended/Deficient BODIPYs and Low-Band-Gap Donor−Acceptor Copolymers for Organic Optoelectronics

Ayse Can, Gi-Seok Choi, Resul Ozdemir, Soyoon Park, Jin Su Park, Yongchul Lee, İbrahim Deneme, Evren Mutlugun, Choongik Kim,* Bumjoon J. Kim,* and Hakan Usta*

Cite This: *ACS Appl. Polym. Mater.* 2022, 4, 1991−2005

Read Online

ACCESS | Metrics & More | Article Recommendations | Supporting Information

ABSTRACT: The realization of π-deficient acceptors and their donor−acceptor copolymers has become a key research focus for the realization of versatile organic optoelectronic materials and devices. Herein, we demonstrate the theoretical design, synthesis, and physicochemical/optoelectronic characterization of two meso-π-extended/deficient BODIPY building blocks (**2OD−T2BDY** and **2OD−TTzBDY**) and a library of donor−acceptor copolymers with low band gap (E_g = 1.30−1.35 eV) based on these building blocks. These building blocks, to the best of our knowledge, are the first examples of BODIPYs with meso-π-extension. A library of BODIPY building blocks with varied meso units/substituents is studied to reveal the meso effects on the semiconducting BODIPY's optoelectronic properties. The building blocks showed favorable π-acceptor electronic/structural properties with meso-π-delocalized and stabilized LUMOs (ca. −3.6 eV) and large ground-state dipole moments of 4.9−5.5 D. Consistent with the theoretical/experimental π-electronic structures, all copolymers functioned as *p*-type semiconductors in field-effect transistors and as donor materials in the bulk heterojunction organic photovoltaics. Power conversion efficiencies of up to 4.4% with a short-circuit current of 12.07 mA cm^{-2} were achieved. This study demonstrates a unique meso-π-extension strategy to realize BODIPYs with favorable π-acceptor properties, and our findings could open up future materials design avenues in various organic optoelectronic applications.

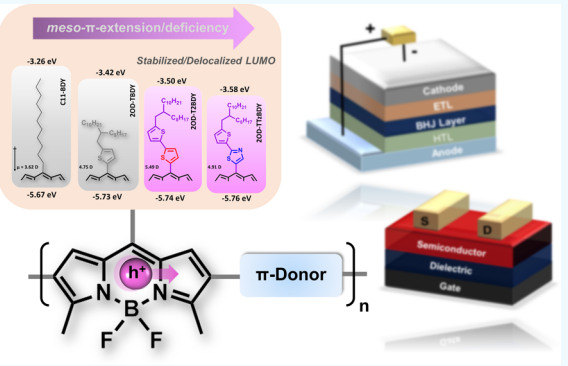

KEYWORDS: *conjugated polymers, BODIPY, organic solar cells, organic semiconductors, LUMO*

INTRODUCTION

Solution-processed bulk heterojunction (BHJ) films of hole-transporting π-conjugated polymers and electron-transporting low-LUMO small molecules are indispensable components of organic solar cells possessing the desirable features of being lightweight and flexible and having roll-to-roll processability.[1−10] A three-dimensional cocontinuous network of these semiconducting materials in BHJ layers has been demonstrated to yield high photon-to-current conversion efficiencies in organic photovoltaics (BHJ-OPVs).[1,11−14] Early studies prior to 2010[15] focused on using functionalized/substituted[16] derivatives of readily available benchmark polymeric π-systems (e.g., poly(thiophene)[17,18] and poly(phenylenevinylene)[19,20]) having a single type of π-electron-rich aromatic unit. Recent studies in the past decade revealed that donor−acceptor (D−A)-type polymer architectures give the best π-electronic structures with regard to optical absorption, exciton dynamics, and charge transport,[11,21,22] leading to remarkable enhancements of the power conversion efficiencies (PCEs) of over 17%.[2,4,23−25] Nevertheless, π-deficient acceptor building blocks in the efficient D−A copolymers still span a limited number of π-frameworks. Some examples of these acceptor building blocks are ester-functionalized thieno[3,4-*b*]thiophene,[26] diketopyrrolopyrrole,[27,28] benzo[1,2-*c*:4,5-*c*′]dithiophene-4,8-dione,[29,30] benzo[*d*][1,2,3]triazole,[31,32] and thieno[3,4-*c*]-pyrrole-4,6-dione.[33,34] Therefore, the design and synthesis of π-electron-deficient acceptor units and their D−A copolymers with proper structural and optoelectronic characteristics are important, especially considering the recent development of many D−A copolymer donors and nonfullerene small molecule/polymer acceptors leading to significant structural versatility and performance improvements.[12,14,35−47] In addition, π-deficient acceptor units and their low-band-gap D−A copolymers could also offer great potential for use in other organic optoelectronic technologies such as near-infrared organic photodetectors and ambipolar transistors.[48−54]

Received: December 18, 2021
Accepted: February 7, 2022
Published: February 16, 2022

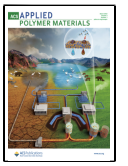

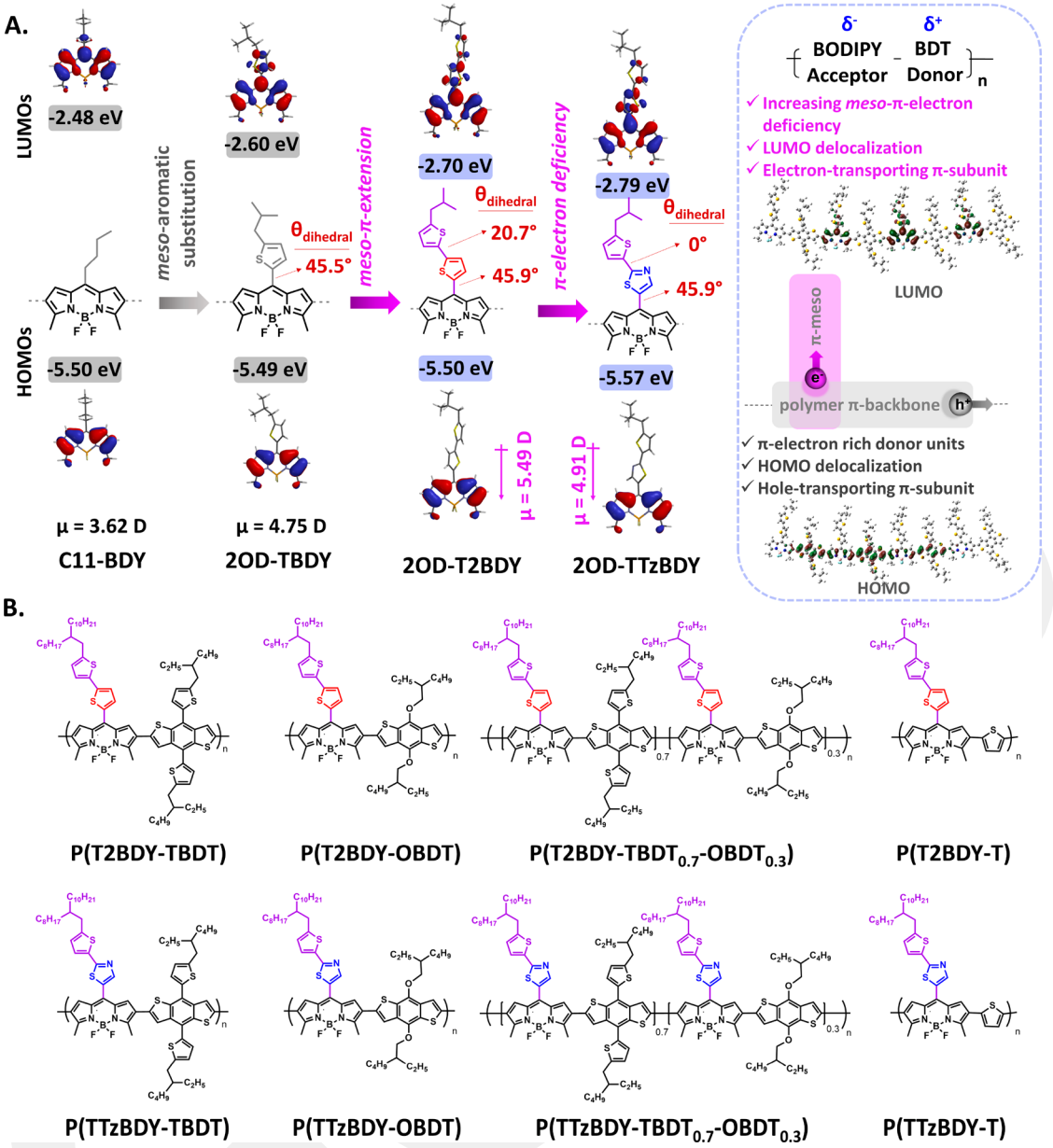

Figure 1. (A) Monomeric models for **C11−BDY** and **2OD−TBDY** developed in our previous studies[58,70] and *meso*-bithiophene-substituted **2OD−T2BDY** and *meso*-thiazole-thiophene-substituted **2OD−TTzBDY** developed in this study. Effect of aromatic substitutions and increasing π-extension/electron deficiency at BODIPY's meso positions on the frontier molecular orbital (HOMO/LUMO) energy levels and topographies, dihedral angles ($\theta_{dihedral}$), and molecular dipole moments (μ) of the BODIPY π core (B3LYP/6-31G** level of theory). Design rationales of the current meso-π-extended **BODIPY−BDT** donor−acceptor copolymers and representative HOMO−LUMO topographies for the tetramer model of **P(T2BDY−TBDT)** (B3LYP/6-31G** level of theory). (B) Chemical structures of the donor−acceptor copolymers **P(T2BDY−TBDT)**, **P(T2BDY−OBDT)**, **P(T2BDY−TBDT$_{0.7}$−OBDT$_{0.3}$)**, **P(T2BDY−T)**, **P(TTzBDY−TBDT)**, **P(TTzBDY−OBDT)**, **P(TTzBDY−TBDT$_{0.7}$−OBDT$_{0.3}$)**, and **P(TTzBDY−T)** developed in this study.

4,4-Difluoro-4-bora-3*a*,4*a*-diaza-*s*-indacene (BODIPY) compounds were first synthesized more than five decades ago, and they have been a key building block in the last 20 years for the realization of functional molecules in fluorescence-based sensing and bioimaging applications.[55] Nonetheless, they have not played a critical role in organic photovoltaics until very recently. In the past few years, significant progress has been made in BODIPY-based D−A copolymers and their implementation in high-performance BHJ-OPVs. Compared to simple alkyl-substituted BODIPYs, *meso*-(hetero)aryl functionalization has provided key advantages. Following the report by Chochos et al. and Kim and Ma et al. giving PCEs of 1−2%[56,57] and our study with PCEs of up to 6.2%,[58] Liu et al.[59] and Bucher et al.[60] very recently demonstrated PCEs of ∼9−10% using *meso*-(hetero)aryl-functionalized BODIPY-based acceptor units in D−A copolymers (Table S1 for the full list of BODIPY-based copolymers in BHJ-OPVs). Previous studies, including our works,[58,61] have demonstrated that BODIPYs yield efficient electron-transport characteristics upon π-conjugation from their meso positions, while 2,6-π-conjugation leads to hole transport. Therefore, *meso*-heteroaryl BODIPY stands out as an ideal monomer for D−A copolymers with a low band gap, yielding a hole-transporting polymer π-backbone upon copolymerization through the 2,6 positions

https://doi.org/10.1021/acsapm.1c01856
ACS Appl. Polym. Mater. 2022, 4, 1991−2005

with electrons delocalizing only on the *meso*-heteroaryl BODIPYs.

We envision that more synthetic effort could be placed on developing *meso*-heteroaryl BODIPYs to further explore their optoelectronic properties and roles in donor−acceptor polymers. Our current research direction herein is to further π extend this *meso*-heteroaryl unit and introduce additional π-electron deficiency by employing 2,2′-bithiophene and 2-(thiophen-2-yl)thiazole conjugation units. Two highly soluble BODIPY-based building blocks (Figure 1, **2OD−T2BDY** and **2OD−TTzBDY**) with strong π-acceptor and favorable structural/electronic properties (e.g., stabilized/delocalized LUMO, large dipole, and meso-π-coplanarity) were designed, synthesized, and fully characterized. These building blocks were synthesized as 2,6-dibromo-substituted monomers to yield hole-transporting D−A copolymers in linear backbone geometries. Upon copolymerization with three different donor comonomers, 2,6-bis(trimethytin)-4,8-bis(5-(2-ethylhexyl)-thiophen-2-yl)benzo[1,2-*b*:4,5-*b*′]dithiophene (**Me_3Sn-$(2EHT)_2$BDT-$SnMe_3$**), 4,8-bis[(2-ethylhexyl)oxy]-2,6-bis-(trimethylstannyl)benzo[1,2-*b*:4,5-*b*′]dithiophene (**Me_3Sn-$(2EHO)_2$BDT-$SnMe_3$**), and 2,5-bis(trimethylstannyl)-thiophene (**Me_3Sn−T-$SnMe_3$**), eight different D−A copolymers were prepared. Four of them, **P(T2BDY−TBDT)**, **P(T2BDY−$TBDT_{0.7}$−$OBDT_{0.3}$)**, **P(TTzBDY−TBDT)**, and **P(TTzBDY−$TBDT_{0.7}$−$OBDT_{0.3}$)**, were highly soluble in common organic solvents, showed low optical band gaps (E_g = 1.30−1.35 eV), and were fully characterized. The semiconducting features were investigated in organic field-effect transistors (OFETs) in a bottom-gate/top-contact geometry, which revealed clear *p*-type charge transport for all copolymers. Photovoltaic devices consisting of these copolymers as donor materials in the BHJ layer showed PCEs of up to 4.40% with a J_{sc} value of 12.07 mA cm^{-2}. To the best of our knowledge, this study shows the first example of meso-π-extended BODIPYs as potential building blocks for developing low-band-gap D−A copolymers for use in photovoltaic and other organic optoelectronic applications. To our knowledge, among the reported BODIPY monomers, the LUMOs (from −3.50 to −3.58 eV) of the current building blocks are the lowest.

RESULTS AND DISCUSSION

Computational Design of the Meso-π-Extended/Deficient BODIPY Acceptors and D−A Copolymers. Meso-π-extended building blocks, **2OD−T2BDY** and **2OD−TTzBDY**, were studied with regard to their structural and electronic characteristics via computational modeling prior to their synthesis by employing isobutyl substituents to represent 2-octyldodecyl chains. Thus, to obtain a complete picture of the structural/electronic effects of *meso*-heteroaryl functionalization and meso-π-extension/deficiency on BODIPYs, calculations ranging from **C11−BDY** with a *meso*-alkyl substitution and **2OD−TBDY** with a single thiophene unit to the current building blocks were performed (Figure 1A). *meso*-Thienyl functionalization delocalizes BODIPY's LUMO, which is localized mainly on the 2,2′-dipyrromethene π-system in **C11−BDY**, toward the meso position and yields an energetic stabilization of 0.12 eV. However, the HOMO wave function topography and energy remain unchanged. Consistent with this original trend, LUMO π-delocalization further extends into the meso positions when "2,2′-bithiophene" and "2-(thiophen-2-yl)thiazole" heteroaryl units were employed, respectively, in the building blocks **2OD−T2BDY** and **2OD−TTzBDY**. In addition, the LUMO energies decrease by ∼0.1−0.2 eV relative to **2OD−TBDY** having a single thiophene unit. Minimal changes were observed in the HOMOs of **C11−BDY**, **2OD−TBDY**, and **2OD−T2BDY** since the corresponding wave functions are localized only on the 2,2′-dipyrromethene π-core with a node at the meso position. While the decrease in LUMO going from **2OD−TBDY** to **2OD−T2BDY** originates purely from meso-π-extension, the energetic stabilization going from **2OD−T2BDY** to **2OD−TTzBDY** is due to the thiazole unit's π-electron deficiency.[62−64] This meso-π-electron deficiency in **2OD−TTzBDY** even decreases the HOMO energy by ∼0.07 eV via a negative inductive ($-I$) effect. The meso-π-extension/π-deficiency was observed to have a minimal effect on the dihedral angles ($\theta_{dihedral}$ = 45.5−45.9°) between the attached *meso*-heteroaryl unit and the highly coplanar dipyrromethane π-core. This indicates that the steric interactions between the five-membered thienyl ring adjacent to the dipyrromethane π-core determines the extent of this intramolecular π-distortion. Note that these dihedral angles are consistent with those ($\theta_{dihedral}$ = 44.9−48.8°) measured in the single-crystal structures of our previously reported BODIPY-based molecular semiconductors.[61,65] On the other hand, a clear difference was observed between the *meso*-heteroaryl unit coplanarities. While the 2-(thiophen-2-yl)thiazole meso unit in **2OD−TTzBDY** is found to adopt a highly coplanar ($\theta_{T-Tz(dihedral)} \approx 0°$) conformation, a larger thiophene−thiophene dihedral angle of 20.7° exists in **2OD−T2BDY**. The planarization of the 2-(thiophen-2-yl)thiazole meso unit is most likely facilitated by replacing "C−H···C−H" repulsions with attractive "N···S" interactions[66] and inducing intramolecular "conformational lock" in which, as suggested by Bronstein et al.,[64,67] the thiazole nitrogen lone pair interacts with the thiophene's adjacent carbon−sulfur antibonding orbital. The ground-state dipole moments of the current BODIPY building blocks (μ = 5.49 D for **2OD−T2BDY** and 4.91 D for **2OD−TTzBDY**) are calculated to be larger than those of simple *meso*-alkyl- or -thienyl-substituted **C11−BDY** (μ = 3.62 D) and **2OD−TBDY** (μ = 4.75 D). Since the positive ends of the dipoles are on the *meso*-heteroaryl units and the dipole moment vectors point toward the 4,4′-difluorine substituents, the increased magnitudes of the ground-state dipole moments, which are among the highest in the literature for a π-acceptor monomeric unit, are clearly a result of the increased dipolar distance and meso unit polarizability. We note that some previous studies have suggested that large dipoles on the π-backbone of D−A copolymers could enhance interchain dipolar interaction energies[68] and facilitate favorable exciton/charge-separation characteristics in photovoltaics.[4,69]

In order to understand whether the favorable electronic properties of the current BODIPY building blocks could be translated into D−A type polymer π-backbones, DFT calculations were performed using the benzodithiophene donor unit for oligomeric model compounds. On the basis of our calculations, the electronic properties of the D−A π-backbone were found to saturate at the tetramer level (Figure S31); thus, we focus on $(D-A)_4$ oligomeric models. As shown in Figures 1A, 4D, S31, and S32, consistent with all of our design rationales discussed earlier and *p*- vs *n*-type semiconductivities observed with BODIPYs in the literature,[58,61] the polymer π-backbones show an extensive delocalization for the HOMO over a number of boron-dipyrromethene and benzodithiophene units whereas the LUMOs are found to be

https://doi.org/10.1021/acsapm.1c01856
ACS Appl. Polym. Mater. 2022, 4, 1991−2005

Scheme 1. Synthesis of Meso-π-Extended/Deficient BODIPY Monomers 2OD−T2BDY−Br_2 and 2OD−TTzBDY−Br_2

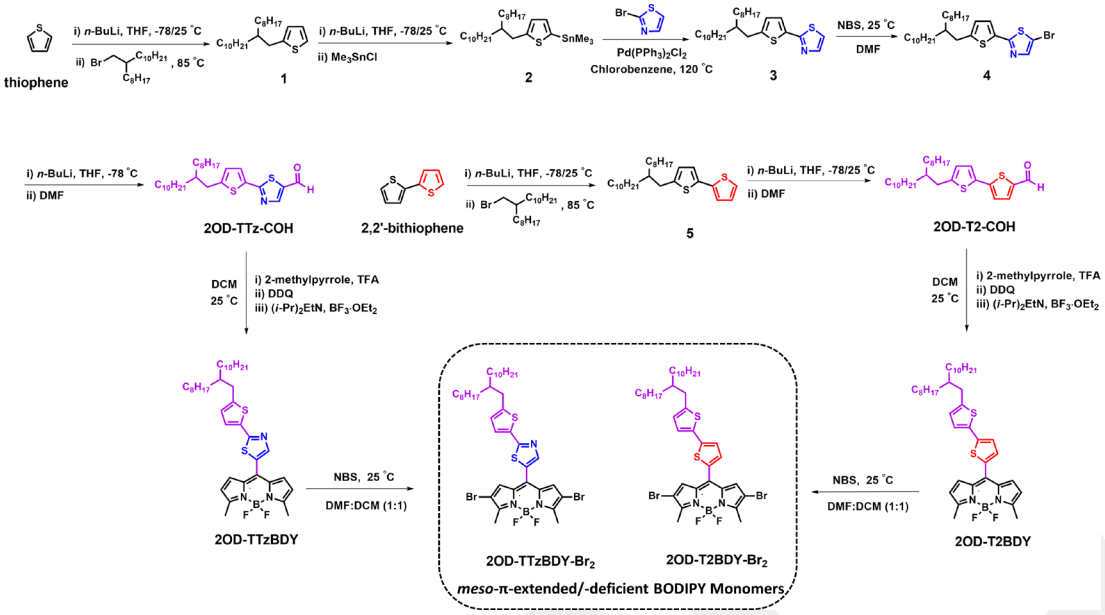

localized on BODIPY with significant contributions from the *meso*-heteroaryl units. This spatial separation observed for the frontier orbital wave functions along with the large dipoles of the BODIPY units and the intrinsic charge-transport characteristics of the BODIPY π-systems (i.e., hole transport along the polymer π-backbone direction and electron transport along the meso-π-direction) are expected to lower the exciton Coulomb binding energy on the polymer backbone and to lead to effective charge-transfer/hole-transport dynamics in bulk heterojunction photovoltaics.[69,71] Going from the BODIPY π-acceptor building blocks to the D−A polymers, while the HOMOs are calculated to increase considerably by ∼0.7 eV, the LUMOs decrease only by ∼0.2 eV (Figures 1A and S32), suggesting a band-gap reduction of ∼0.5 eV after polymerization. These energetic changes are consistent with the polymer wave function topographies indicating the significant contribution of π-electron-rich donor units in the HOMOs. Finally, in the structural design of the current building blocks, sterically encumbered swallow-tailed 2-octyldodecyl substituents are positioned further away from the semiconducting D−A π-system as a natural outcome of the meso-π-extension. The physical separation between σ-insulating alkyl chains and D−A π-system via side-chain engineering has been demonstrated to yield very efficient charge-transport characteristics in semiconducting copolymers.[72]

Synthesis and Structural−Optoelectronic Characterization of the Meso-π-Extended/Deficient BODIPY Acceptors. The syntheses of the building blocks **2OD−T2BDY** and **2OD−TTzBDY** and their corresponding dibromo-functionalized monomers are shown in Scheme 1. The carboxaldehyde compound **2OD−T2-COH** was prepared in two steps from readily available 2,2′-bithiophene by first substituting the 5′ position with 2-octyldodecyl via lithiation/alkylation (**5** in 43.9% yield) and then functionalizing the 5 position of **5** with carboxaldehyde via lithiation/DMF (**2OD−T2-COH** in 63.4% yield). The synthesis of the other carboxaldehyde, **2OD−TTz-COH**, involved more steps due to its asymmetrical chemical structure. The synthesis of this carboxaldehyde started with lithiation/alkylation of readily available thiophene at the 5 position (**1** in 41% yield), which was then stannylated at the 2 position to give **2** in 96% yield. Compound **2** was next coupled with 2-bromothiazole via a Stille cross-coupling reaction using $Pd(PPh_3)_2Cl_2$/chlorobenzene as the catalyst/solvent system, which yielded **3** in 58% yield. At this point, we initially attempted the synthesis of **2OD−TTz-COH** directly from **3** via lithiation/DMF. However, a mixture of carboxaldehyde-functionalized compounds (three different −CO**H** peaks in the ^{1}H NMR spectrum) was obtained, which was found to be inseparable to yield the desired product. This is attributed to the asymmetrical structure of **3** and the presence of an electron-withdrawing sp^2-hybridized nitrogen activating several carbon sites for lithiation as previously reported.[62,73] Therefore, first, a highly selective electrophilic bromination was employed on **3** with NBS to obtain **4** (84% yield), which was then lithiated at −78 °C via a metal−halogen exchange reaction and reacted with DMF to yield **2OD−TTz-COH** (33% yield). The boron−dipyrromethene π-cores **2OD−T2BDY** and **2OD−TTzBDY** were prepared in 19−24% yields by reacting **2OD−T2-COH** and **2OD−TTz-COH**, respectively, with 2-methylpyrrole in trifluoroacetic acid (TFA) (catalytic amount), followed by subsequent oxidation with 2,3-dichloro-5,6-dicyano-1,4-benzoquinone (DDQ) and coordination with trifluoroborane dietherate (BF_3·OEt_2). Highly selective 2,6-dibrominations on the BODIPY π-cores were realized with *N*-bromosuccinimide (NBS) to afford **2OD−T2BDY−Br_2** and **2OD−TTzBDY−Br_2** in 86% and 61% yields, respectively. The molecular structures/purities of the intermediate compounds and the BODIPY monomers were evaluated by ^{1}H/^{13}C NMR spectroscopy (Figures S1−S6, S8, S9, S11−S17, S19, and S20, Supporting Information), atmospheric pressure chemical ionization mass spectrometry (APCI-MS) (Figures S7, S10, S18, and S21, Supporting Information), and elemental analysis. To reveal the optoelectronic effects of meso-π-extension/deficiency in the current π-acceptor building blocks and to make delicate comparisons, we also synthesized our previously reported BODIPY π-acceptor building blocks **C11−BDY** and

https://doi.org/10.1021/acsapm.1c01856
ACS Appl. Polym. Mater. 2022, 4, 1991−2005

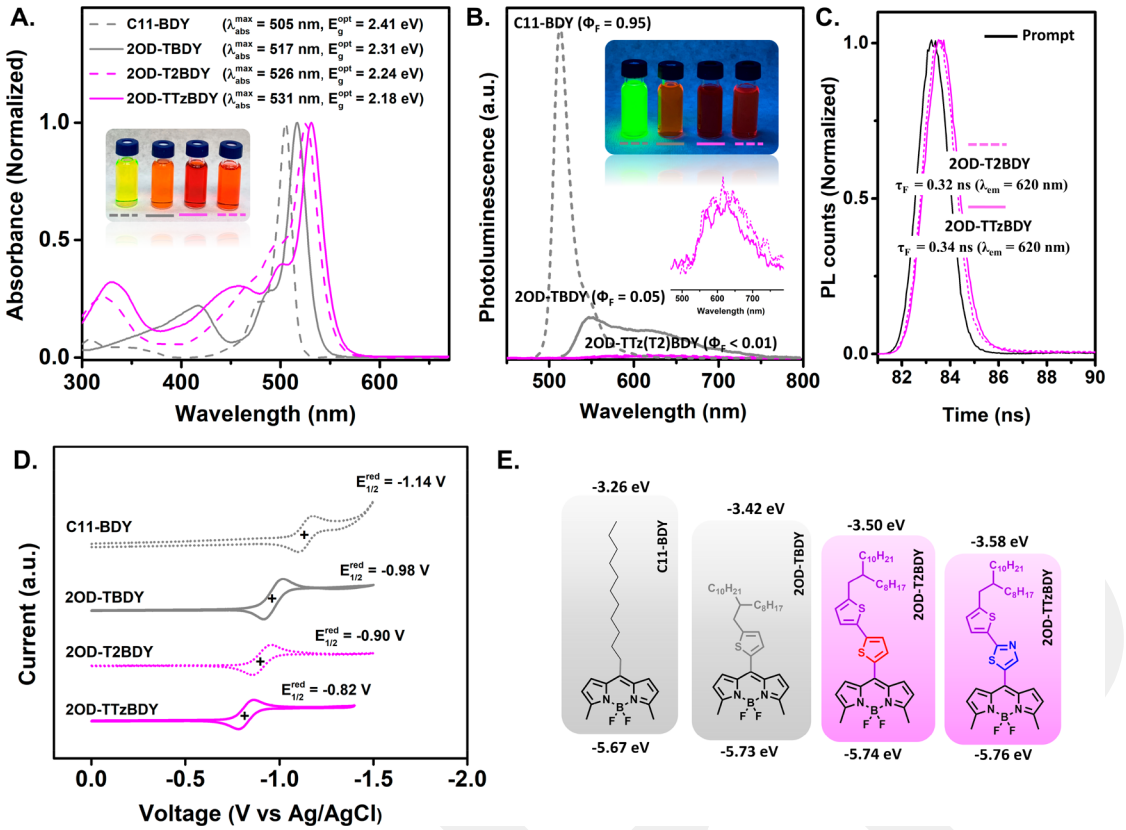

Figure 2. (A) Optical absorption spectra in dichloromethane (1.0×10^{-5} M), (B) photoluminescence spectra ($\lambda_{exc} \approx \lambda_{abs}^{max}$) in dichloromethane ($1.0 \times 10^{-5}$ M) and calculated fluorescence quantum yields (Φ_F), (C) transient photoluminescence decay profiles measured in dichloromethane (1.0×10^{-5} M) at 620 nm upon excitation at 390 nm and measured fluorescence lifetimes (τ_F), (D) cyclic voltammograms vs Ag/AgCl (3.0 M NaCl) (in 0.1 M $Bu_4N^+PF_6^-$ dichloromethane, scan rate = 50 mV s^{-1}), and (E) experimentally determined frontier molecular orbital energies for **C11−BDY**, **2OD−TBDY**, **2OD−T2BDY**, and **2OD−TTzBDY**. (Insets in A and B) Optical images of BODIPY π-acceptor molecules in dichloromethane solution under room light and optical excitation, respectively.

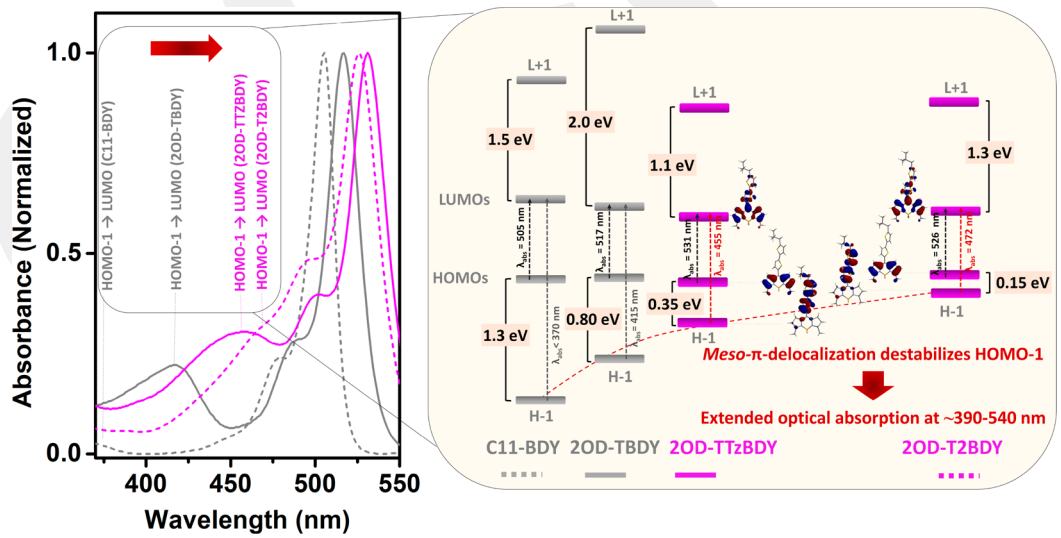

Figure 3. Optical absorption spectra of **C11−BDY**, **2OD−TBDY**, **2OD−T2BDY**, and **2OD−TTzBDY** in dichloromethane (1.0×10^{-5} M) showing higher energy optical transitions in the ~390−540 nm spectral region next to the main $\pi \rightarrow \pi^*$ transitions, and the corresponding HOMO−1, HOMO, LUMO, and LUMO+1 molecular orbital energies and wave function topographies (B3LYP/6-31G** level of theory). The red dashed line is a guide to the eye to illustrate the HOMO−1 destabilization for **C11−BDY** → **2OD−TBDY** → **2OD−TTzBDY** → **2OD−T2BDY**.

2OD−TBDY in accordance with the earlier procedures (Supporting Information for synthesis details).[58,70]

The optical and electrochemical characteristics of the meso-π-extended/deficient BODIPY π-acceptor building blocks **2OD−T2BDY** and **2OD−TTzBDY** in combination with the

https://doi.org/10.1021/acsapm.1c01856
ACS Appl. Polym. Mater. 2022, 4, 1991−2005

Scheme 2. Synthesis of D−A Copolymers P(T2BDY−TBDT), P(T2BDY−OBDT), P(T2BDY−T), P(T2BDY−TBDT$_{0.7}$−OBDT$_{0.3}$), P(TTzBDY−TBDT), P(TTzBDY−OBDT), P(TTzBDY−T), and P(TTzBDY−TBDT$_{0.7}$−OBDT$_{0.3}$) from the Meso-π-Extended/Deficient BODIPY Monomers 2OD−TTzBDY−Br$_2$ and 2OD−T2BDY−Br$_2$

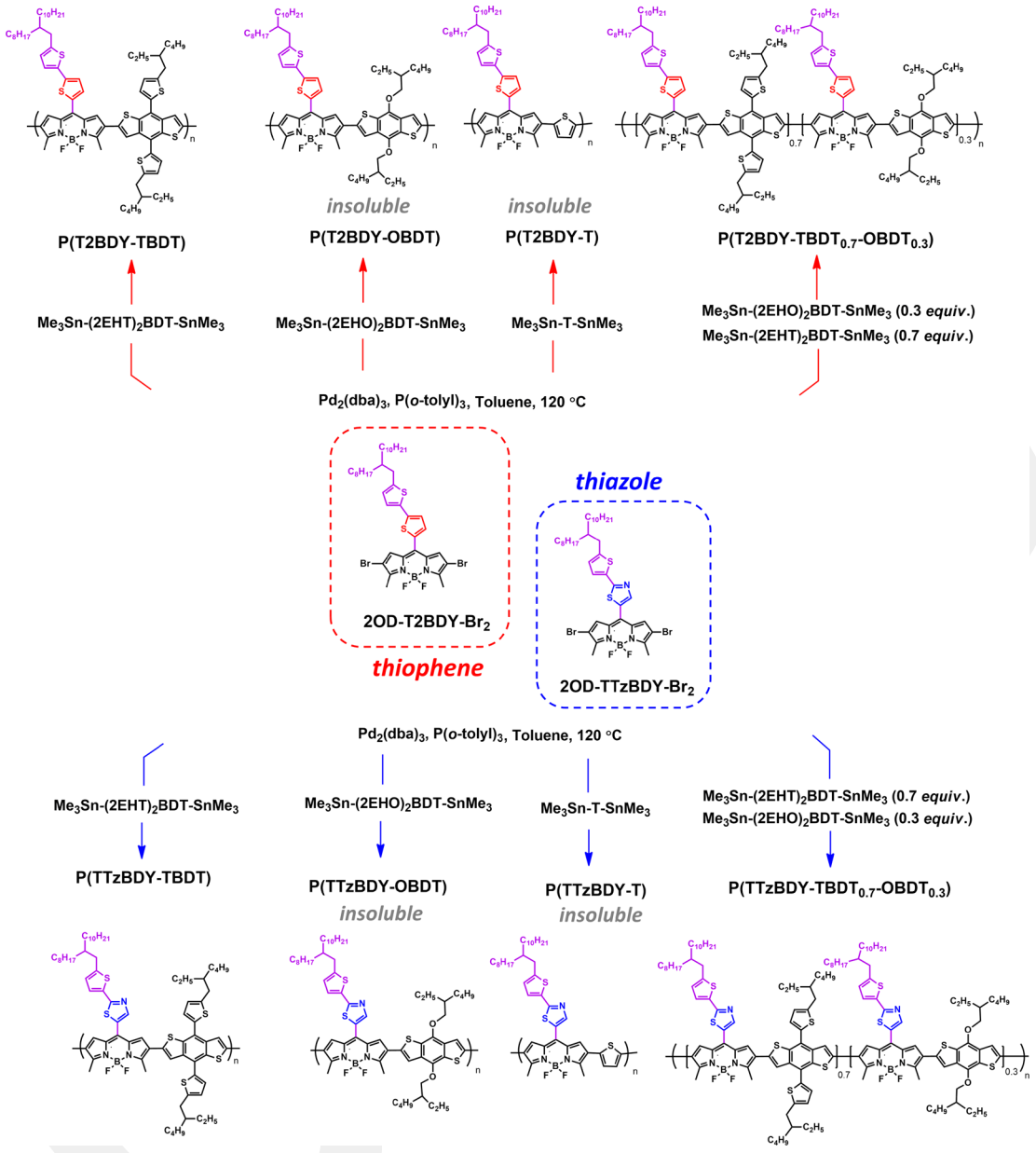

meso-alkyl- and -heteroaryl-functionalized counterparts **C11−BDY** and **2OD−TBDY** were studied in solution (dichloromethane, 1.0 × 10^{-5} M) by UV−vis absorption and steady-state/time-resolved photoluminescence spectroscopies and cyclic voltammetry. As shown in Figure 2A, the current building blocks exhibit the characteristic intense $\pi-\pi^*$ ($S_0 \rightarrow S_1$) absorption peak of the BODIPY π-system with λ_{max} values at 526 (ε = 1.60 × 10^4 M^{-1} cm^{-1}) and 531 nm (ε = 1.50 × 10^4 M^{-1} cm^{-1}), respectively, and the out-of-plane vibronic features ($\lambda_{abs(0-1)}$ and $\lambda_{abs(0-2)}$) at ∼1100−1200 cm^{-1} from the absorption maxima ($\lambda_{abs(0-0)}$). The optical band gaps (E_g^{opt}) are estimated from the low-energy band edges as 2.24 and 2.18 eV, respectively. Most importantly, in addition to BODIPY's main absorption peaks at 526−531 nm, relatively intense absorption bands with λ_{max} at 455 and 472 nm ($\varepsilon \approx$ 30−35% of the main absorption peak), respectively, appear in the current BODIPY building blocks. Note that the *meso*-alkyl substituent in **C11−BDY** yields the second relatively low intensity (ε < 7% of the main absorption peak) absorption peak below 370 nm, and the *meso*-thienyl unit (i.e., a single heteroaryl ring) in **2OD−TBDY** was able to shift this absorption only to a λ_{max} value of 415 nm.

In order to reveal the origin of the optical absorption extension in the ∼390−540 nm spectral region, detailed analysis of the frontier molecular orbitals including the HOMO−1 and LUMO+1 was performed. As shown in Figure 3, since the LUMO+1 orbitals lie at very high energies relative to the LUMOs (ΔE = 1.1−2.0 eV), they could yield optical transitions only at <350−400 nm. However, the HOMO−1 orbitals are identified to be energetically close (ΔE = 0.15−0.35 eV) to the HOMOs. Since the HOMO−1 wave functions are exclusively on the *meso*-heteroaryl units, they are largely

https://doi.org/10.1021/acsapm.1c01856
ACS Appl. Polym. Mater. 2022, 4, 1991−2005

destabilized as compared to **C11−BDY** and **2OD−TBDY** and involved in the formation of optical transitions in the ∼390−540 nm spectral region.[74] As shown in Figure 3, while the HOMO/HOMO−1 energy difference in **2OD−T2BDY** is 0.15 eV, π-electron deficiency of the thiazole unit in **2OD−TTzBDY** stabilizes the HOMO−1, yielding an energetic separation of 0.35 eV with the HOMO level. It is amazing that the HOMO/HOMO−1 energy differences in the current building blocks coincide well with the observed absorption peaks at 455 (0.37 eV from the main absorption peak of **2OD−TTzBDY** at 531 nm) and at 472 nm (0.19 eV from the main absorption peak of **2OD−T2BDY** at 526 nm). When compared with **C11−BDY** and **2OD−TBDY**, the optical transitions and the band gaps of **2OD−T2BDY** and **2OD−TTzBDY** are bathochromically shifted by ∼0.10−0.25 eV, and relatively strong optical transitions are formed in the ∼390−540 nm spectral region, which are undoubtedly the result of meso-π-extension in the current BODIPYs and indicate favorable optical absorption characteristics for use in photovoltaics.

The electrochemical properties were studied via cyclic voltammetry. In order to grasp subtle energetic changes, all four BODIPY building blocks were studied in the same electrochemical setup in 0.1 M $TBAPF_6$ dichloromethane solution against Ag/AgCl (3.0 M NaCl) reference electrode. While **C11−BDY** and **2OD−TBDY** show reversible reduction peaks at −1.14 and −0.98 V, respectively, anodically shifted (ΔV = 0.08−0.32 V) reversible reductions are observed for **2OD−T2BDY** ($E^{red}_{1/2}$ = −0.90 V vs Ag/AgCl) and **2OD−TTzBDY** ($E^{red}_{1/2}$ = −0.82 V vs Ag/AgCl) as a result of their better π-acceptor characteristics. Significantly low LUMO energies (E_{LUMO}'s) of −3.50 and −3.58 eV, respectively, are estimated. The low E_{LUMO}'s and the reversibility of the reduction processes indicate the highly stable *n*-doping/undoping behavior of the current building blocks. The HOMO energies (E_{HOMO}) are estimated either using measured E_{LUMO}/E_g^{opt} values in the "$E_{HOMO} = E_{LUMO} - E_g^{opt}$" equation or measuring irreversible oxidation peaks (Figure S24), both of which give comparable values. The HOMOs are estimated to be −5.74 and −5.76 eV for **2OD−T2BDY** and **2OD−TTzBDY**, respectively. The electrochemical band gaps are measured to be 2.19 (E_g^{opt} = 2.24 eV) and 2.16 eV (E_g^{opt} = 2.18 eV) for **2OD−T2BDY** and **2OD−TTzBDY**, respectively. Finally, steady-state and time-resolved photoluminescence studies were performed to understand the excited-state behaviors. The photoluminescence spectra of **2OD−T2BDY** and **2OD−TTzBDY** in dichloromethane (ε = 8.93) solutions (Figure 2B) exhibit very low intensity broad emission peaks with maxima at ∼620 nm (very large Stokes shifts of ∼90−100 nm), and the corresponding fluorescence quantum yields (Φ_F) are measured to be very low (Φ_F < 0.01). These emission characteristics remain the same even in nonpolar solvents such as cyclohexanes (ε = 2.02) and toluene (ε = 2.38). The transient photoluminescence decay profiles in dichloromethane solutions at 620 nm (λ_{exc} = 390 nm) (Figure 2C) show a single-exponential decay with very short lifetimes of 0.32 (for **2OD−T2BDY**) and 0.34 ns (for **2OD−TTzBDY**). On the other hand, **2OD−TBDY** with one *meso*-heteroaryl unit shows two emission peaks in dichloromethane at 540 (Stokes shift ≈ 23 nm) and 620 nm (Stokes shift ≈ 103 nm). The relatively stronger emission peak observed at 540 nm indicates that the LE-dominated excited state is still radiative when a single heteroaryl unit is meso attached to BODIPY, and the corresponding fluorescence quantum yield is relatively larger (Φ_F = 0.05) as compared to the current meso-π-extended BODIPYs. When the *meso*-heteroaryl unit is completely removed and the alkyl chain is placed instead, a very intense fluorescence emission (Φ_F = 0.95) with a small Stokes shift of ∼7 nm is observed for **C11−BDY**, which originates from a purely LE-dominated excited state.[55] The observed significantly red-shifted broad emission peaks, very low quantum yields, and fast decay kinetics are very different than those of characteristic BODIPY emissions.[61] These observations together clearly indicate that meso-π-extension/deficiency facilitates CT-excited-state formation and could induce a very favorable exciton dissociation pathway in the excited state as compared with single-heteroaryl and alkyl meso-substituted BODIPYs. Amazingly, all optoelectronic characterization results are in line with the aforementioned theoretical calculations (Figure 1) and point to the favorable π-acceptor characteristics of the current building blocks for use in D−A copolymers in BHJ-OPVs.

Synthesis and Structural−Physicochemical−Optoelectronic Characterization of the D−A Copolymers. As shown in Scheme 2, eight different donor−acceptor copolymers **P(T2BDY−TBDT)**, **P(T2BDY−OBDT)**, **P(T2BDY−T)**, **P(T2BDY−TBDT$_{0.7}$−OBDT$_{0.3}$)**, **P(TTzBDY−TBDT)**, **P(TTzBDY−OBDT)**, **P(TTzBDY−T)**, and **P(TTzBDY−TBDT$_{0.7}$−OBDT$_{0.3}$)** based on the current meso-π-extended/deficient BODIPY acceptor building blocks were synthesized via Stille copolymerization reactions of **2OD−TTzBDY−Br$_2$** and **2OD−T2BDY−Br$_2$** with three different donor monomers, 2,6-bis(trimethytin)-4,8-bis(5-(2-ethylhexyl)thiophen-2-yl)-benzo[1,2-*b*:4,5-*b*′]dithiophene (**Me$_3$Sn-(2EHT)$_2$BDT-SnMe$_3$**), 4,8-bis[(2-ethylhexyl)oxy]-2,6-bis(trimethylstannyl)-benzo[1,2-*b*:4,5-*b*′]dithiophene (**Me$_3$Sn-(2EHO)$_2$BDT-SnMe$_3$**), and 2,5-bis(trimethylstannyl)thiophene (**Me$_3$Sn−T-SnMe$_3$**). The reactions were carried out in toluene using $Pd_2(dba)_3/P(o\text{-tolyl})_3$ (catalyst/ligand) at 120 °C, and the copolymers were obtained after Soxhlet extractions as dark-colored solids. The solubility behaviors of the copolymers were found to be completely different for **(2EHT)$_2$BDT** and **(2EHO)$_2$BDT** donors. When **(2EHT)$_2$BDT** is used as the comonomer, **P(T2BDY−TBDT)** and **P(TTzBDY−TBDT)** were obtained in 72% and 80% yields, respectively, as highly soluble solids; however, **(2EHO)$_2$BDT** and **T** comonomers yielded completely insoluble copolymers (i.e., **P(T2BDY−OBDT)**, **P(T2BDY−T)**, **P(TTzBDY−OBDT)**, and **P-(TTzBDY−T)**). Even aromatic solvents such as toluene and chlorobenzene did not dissolve these copolymers at elevated temperatures (>100 °C). When the solubility of **P(T2BDY−T)** is compared with our previously reported copolymer **P(TBDY−T)**[58] that has the same donor/substituent system, it is evident that meso-π-extension on the BODIPY acceptor unit significantly decreases the solubility. On the other hand, the observed sharp decrease in solubility going from **TBDT** comonomer to **OBDT**, despite the presence of the same 2-ethylhexyl chains, most likely reflects the absence of flexible, polarizable thienyl units at the 4,8 positions of the BDT unit and formation of a stronger donor−acceptor π-electronic structure in **P(T2BDY−OBDT)** and **P(TTzBDY−OBDT)**. Therefore, in order to incorporate the π-electron-rich **(2EHO)$_2$BDT** donor unit into the D−A copolymer backbone, random copolymerizations[75] were performed using the aforementioned copolymerization protocol with 0.7 equiv of **(2EHT)$_2$BDT** and 0.3 equiv of **(2EHO)$_2$BDT**. Soluble

https://doi.org/10.1021/acsapm.1c01856
ACS Appl. Polym. Mater. 2022, 4, 1991−2005

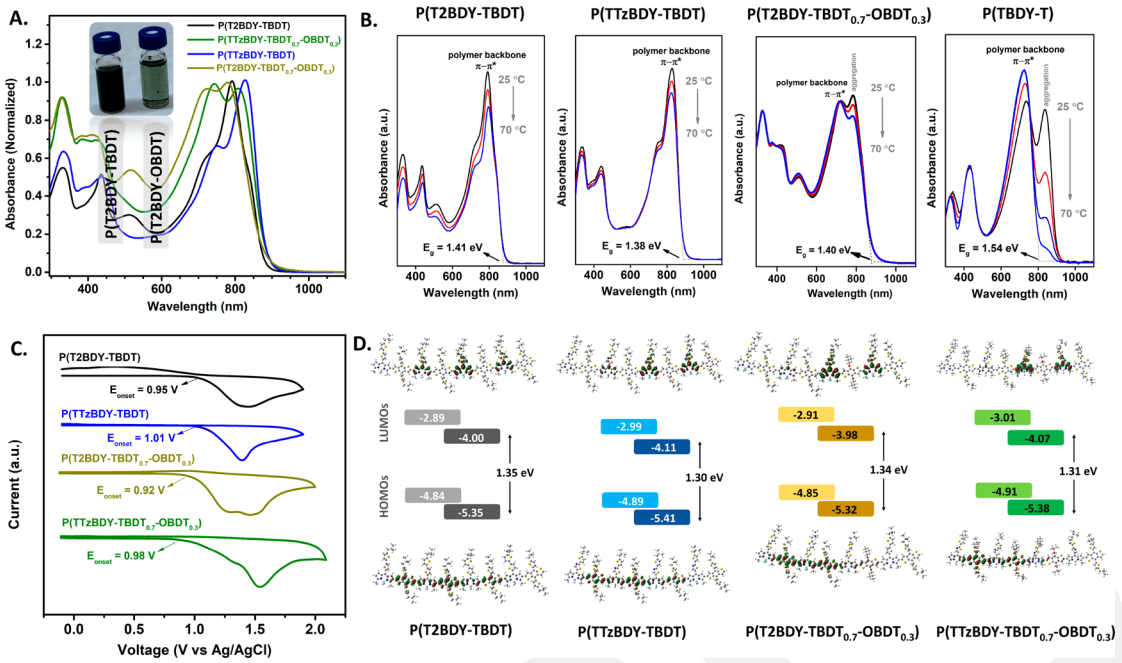

Figure 4. (A) Optical absorption spectra in chloroform (1.0×10^{-5} M). (B) Temperature-dependent (from 25 to 70 °C) UV–vis absorption spectra in toluene solutions (peak intensities in **P(T2BDY–TBDT)** and **P(TTzBDY–TBDT)** are intentionally modified to clarify the spectra at different temperatures). (C) Cyclic voltammograms as thin films vs Ag/AgCl (3.0 M NaCl) (in 0.1 M $Bu_4N^+PF_6^-$ acetonitrile, scan rate = 50 mV s^{-1}). (D) Energy diagrams showing theoretically calculated (light colors) and experimentally estimated (dark colors) HOMO–LUMO frontier orbital energy levels and topographies for the tetramer model compounds for **P(T2BDY–TBDT)**, **P(TTzBDY–TBDT)**, **P(T2BDY–TBDT$_{0.7}$–OBDT$_{0.3}$)**, and **P(TTzBDY–TBDT$_{0.7}$–OBDT$_{0.3}$)**. Note that **P(TBDY–T)**[58] in B is our previously reported BODIPY-based copolymer, and its temperature-dependent UV–vis absorption spectra are shown here for comparison. (Inset in A) Optical images of **P(T2BDY–TBDT)** (completely dissolved) and **P(T2BDY–OBDT)** (suspended as a solid) polymers in chloroform solution.

P(T2BDY–TBDT$_{0.7}$–OBDT$_{0.3}$) and **P(TTzBDY–TBDT$_{0.7}$–OBDT$_{0.3}$)** copolymer solids were then obtained in 46% and 14% yields, respectively. It is noteworthy that the yields for the obtained soluble copolymer solids become much lower (from 72–80% to 14–46%) when the **TBDT** comonomer is replaced with **OBDT**. The copolymer purities were evaluated by ^{1}H NMR spectroscopy (Figures S25, S26, S27, and S28) and elemental analysis. The molecular weights were determined in THF by gel permeation chromatography (GPC) against polystyrene standards. Number-average molecular weights (M_n) of 30 073 (PDI = 2.83), 29 720 (PDI = 4.15), 10 815 (PDI = 2.54), and 9650 Da (PDI = 2.31) were measured for **P(T2BDY–TBDT)**, **P(TTzBDY–TBDT)**, **P(T2BDY–TBDT$_{0.7}$–OBDT$_{0.3}$)**, and **P(TTzBDY–TBDT$_{0.7}$–OBDT$_{0.3}$)**, respectively. The good solubility of these copolymers has enabled the solution-based fabrication of bulk heterojunction thin films for use in photovoltaic devices. The thermal decomposition onset temperatures (5% mass loss based on thermogravimetric analysis) were measured at 320–371 °C for all copolymers (Figure S29), which indicates good thermal stabilities. No evident phase transitions were observed for all copolymers by differential scanning calorimetry (DSC), which is consistent with our previously developed BODIPY copolymers.[58]

The optical absorption properties of the copolymers were evaluated by UV–vis absorption spectroscopy in chloroform solution (1.0×10^{-5} M) and as thin films. As shown in Figure 4A, the copolymers exhibit two low-energy absorption maxima in the near-IR spectral region at 793/731 nm for **P(T2BDY–TBDT)**, 826/748 nm for **P(TTzBDY–TBDT)**, 780/721 nm for **P(T2BDY–TBDT$_{0.7}$–OBDT$_{0.3}$)**, and 807/743 nm for **P(TTzBDY–TBDT$_{0.7}$–OBDT$_{0.3}$)** in chloroform solution, which were found to remain the same with varied solvent polarities (Figure S30A). When the origin of the two-peak absorption profiles was studied via temperature-dependent (Figures 4B and S30B) and solvent–nonsolvent (chloroform–ethanol) mixture (Figure S30D) UV–vis absorption spectra, while no spectral changes were observed for **P(T2BDY–TBDT)** and **P(TTzBDY–TBDT)**, random copolymers **P(T2BDY–TBDT$_{0.7}$–OBDT$_{0.3}$)** and **P(TTzBDY–TBDT$_{0.7}$–OBDT$_{0.3}$)** showed changes in the relative intensities of the two peaks. The low-energy peaks for these two random copolymers were found to decrease with temperature and increase by adding nonsolvent. Similar to our previously reported copolymer **P(TBDY–T)** (spectra on the right in Figures 4B and S30D), the low-energy peaks for **(T2BDY–TBDT$_{0.7}$–OBDT$_{0.3}$)** and **P(TTzBDY–TBDT$_{0.7}$–OBDT$_{0.3}$)** are assigned to electronic transitions in the aggregated (enhanced π-coherence) polymer chains.[58] On the basis of these UV–vis absorption profiles, it is evident that the addition of π-electron-rich **OBDT** units into **P(T2BDY–TBDT)** and **P(TTzBDY–TBDT)** enhances the π-aggregation tendency of the polymer backbones in the random copolymers. This is also consistent with the observed decreases in solubility going from the **TBDT** to the **OBDT** donor unit. On the other hand, for **P(T2BDY–TBDT)** and **P(TTzBDY–TBDT)**, the low-energy peaks are assigned to the π–π^* ($S_0 \rightarrow S_1$) transition of the disaggregated (isolated) polymer chains and the shoulder peaks (at ~1100–1200 cm^{-1} from the absorption maxima) to the vibronic features. The optical band gaps (E_g's) in solution are estimated from the low-energy band edges as 1.38–1.41 eV for all copolymers. Note that matching with the **2OD–TTzBDY**'s

https://doi.org/10.1021/acsapm.1c01856
ACS Appl. Polym. Mater. 2022, 4, 1991–2005

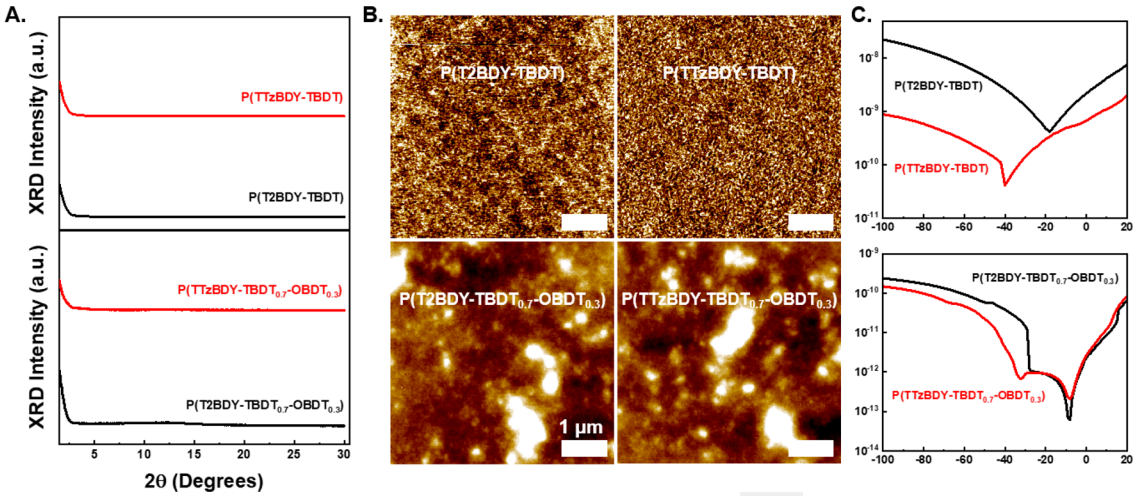

Figure 5. (A) θ–2θ X-ray diffraction (XRD) profiles and (B) AFM topographic images for thin films of **P(T2BDY–TBDT)**, **P(TTzBDY–TBDT)**, **P(T2BDY–TBDT$_{0.7}$–OBDT$_{0.3}$)**, and **P(TTzBDY–TBDT$_{0.7}$–OBDT$_{0.3}$)**. (C) Transfer curves showing *p*-type characteristics (V_{DS} = −100 V) for (BG/TC) OFET devices fabricated with spin-coated copolymer thin films.

stronger π-electron deficiency, bathochromically shifted absorption profiles are recorded in **P(TTzBDY–TBDT)** and **P(TTzBDY–TBDT$_{0.7}$–OBDT$_{0.3}$)** as compared with **P(T2BDY–TBDT)** and **P(T2BDY–TBDT$_{0.7}$–OBDT$_{0.3}$)**. When the current copolymers are compared with our previously reported structurally related copolymer **P(TBDY–T)**, the absorption maxima are significantly red shifted ($\Delta\lambda_{max}$ = 58 and 91 nm) and the optical band gaps are lower (E_g for **P(TBDY–T)** = 1.54 eV). This points to the favorable electronic/structural properties of the current meso-π-extended/deficient BODIPY acceptors and π-electron-rich TBDT/OBDT donor units. Upon copolymerization through the BODIPY's 2,6 positions, the optical absorption profiles shift to the near-IR region ($\Delta\lambda_{max} \approx$ 270–300 nm and $\Delta E_g \approx$ 0.8–0.9 eV), indicating highly extended π-electronic communication in the current copolymer π-backbones with a strong donor–acceptor nature. Also, both the HOMO and the LUMO energies are (de)stabilized by ∼0.4–0.5 eV upon copolymerization (vide infra). Introduction of the π-electron rich **OBDT** donors into the **P(T2BDY–TBDT)** and **P(TTzBDY–TBDT)** backbones resulted in higher relative absorptions for the peaks located to the higher energy end of the main absorption peaks. This leads to more favorable absorption profiles in the visible spectral region for the random copolymers. The absorption maxima for polymer thin films are ∼14–26 nm red shifted as compared to those in solution (Figure S30C), and the solid-state optical band gaps are estimated to be 1.35, 1.30, 1.34, and 1.31 eV for **P(T2BDY–TBDT)**, **P(TTzBDY–TBDT)**, **P(T2BDY–TBDT$_{0.7}$–OBDT$_{0.3}$)**, and **P(TTzBDY–TBDT$_{0.7}$–OBDT$_{0.3}$)**, respectively. As shown in Figure 4C, electrochemical characterization of the drop-casted copolymer films on platinum electrodes shows nonreversible oxidation peaks with onset potentials of 0.95 (vs Ag/AgCl) and 1.01 V (vs Ag/AgCl) for **P(T2BDY–TBDT)** and **P(TTzBDY–TBDT)**, respectively. When π-electron-rich **OBDT** units are introduced, the onset potentials shift to 0.92 (vs Ag/AgCl) and 0.98 V (vs Ag/AgCl) for **P(T2BDY–TBDT$_{0.7}$–OBDT$_{0.3}$)** and **P(TTzBDY–TBDT$_{0.7}$–OBDT$_{0.3}$)**, respectively. The solid-state HOMO/LUMO energies are estimated to be −5.35/−4.00, −5.41/−4.11, −5.32/−3.98, and −5.38/−4.07 eV, respectively. All of these results correlate well with the theoretically calculated frontier orbital energies on the tetramer model compounds and also reflect the structural changes in the BODIPY's meso position and the polymer π-backbones (Figures 4D and S32).

Thin-Film Fabrication, Characterization, and Field-Effect Transistor Devices. In order to reveal the charge-transport characteristics of the four BODIPY-based D–A copolymers **P(T2BDY–TBDT)**, **P(TTzBDY–TBDT)**, **P(T2BDY–TBDT$_{0.7}$–OBDT$_{0.3}$)**, and **P(TTzBDY–TBDT$_{0.7}$–OBDT$_{0.3}$)**, OFETs in a bottom-gate/top-contact (BG/TC) device architecture were fabricated and studied. The polymer thin films (∼50–60 nm) were deposited onto PS-brush-treated n^{++}-Si/SiO_2 (300 nm) via spin-coating polymer solutions (5 mg/mL) in chloroform. PS-brush-modified substrates were employed in order to realize an efficient interface between the semiconductor and the dielectric layers.[76,77] The surface morphology and thin-film microstructure of the spin-coated polymeric semiconductor thin films were studied by atomic force microscopy (AFM) and θ–2θ X-ray diffraction (XRD). As shown in Figure 5A, no distinct diffraction peaks were observed, especially in the low-angle region (2θ < 10°), for all copolymer thin films, which indicates the lack of long-range ordering and lamellar stacking in the out-of-plane direction, most likely due to the presence of bulky swallow-tailed alkyl substituents both on the BODIPY (2-octyldodecyl) and on the donor π-units (2-ethylhexyl).[58] Consistent with the XRD characterization results, thin films of **P(T2BDY–TBDT)** and **P(TTzBDY–TBDT)** exhibited homogeneous morphologies of highly interconnected nodular-like domains (∼60–200 nm) with a low root-mean-square (rms) roughness of ∼0.6 nm (for a 5.0 μm × 5.0 μm scan area). On the other hand, thin films of **P(T2BDY–TBDT$_{0.7}$–OBDT$_{0.3}$)** and **P(TTzBDY–TBDT$_{0.7}$–OBDT$_{0.3}$)** exhibited relatively smooth surfaces with a few small agglomerates and a slightly larger rms roughness of ∼1.7 nm (Figure 5B). The current–voltage characterizations performed under ambient conditions showed that all of the current BODIPY-based D–A copolymers are *p*-type semiconductors with clear hole-transport characteristics. This is consistent with the design rationales of these copolymers (i.e., 2,6-π-extension along the D–A backbone) and their HOMO energy levels (from −5.41 to −5.29 eV). As shown in Figure 5C, the alternating copolymers **P(T2BDY–TBDT)** and **P(TTzBDY–TBDT)** showed hole mobilities of

https://doi.org/10.1021/acsapm.1c01856
ACS Appl. Polym. Mater. 2022, 4, 1991–2005

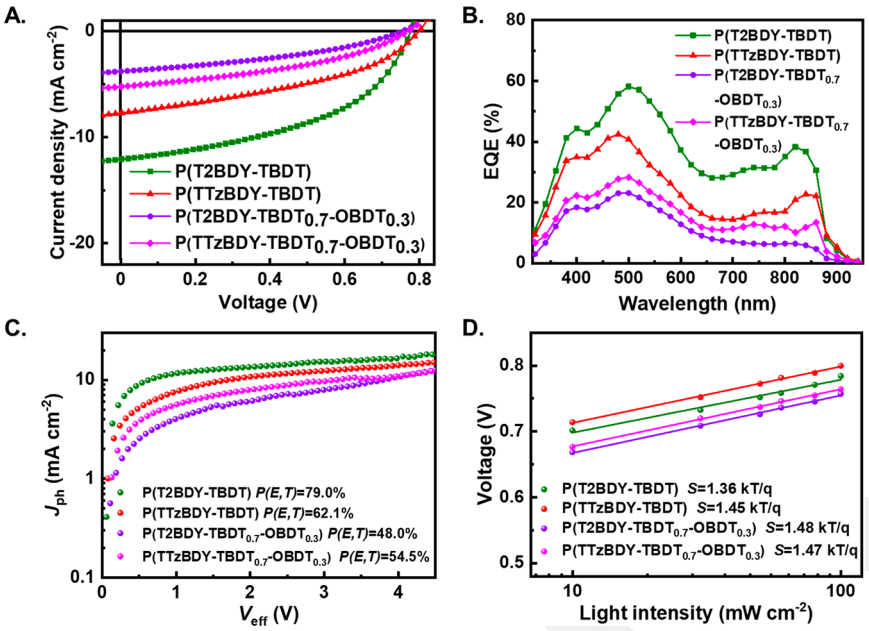

Figure 6. (A) Current density−voltage (J−V) curves, (B) external quantum efficiency (EQE) curves, (C) exciton dissociation probabilities ($P(E,T)$ s), and (D) P_{light}-dependent V_{oc} characteristics for BHJ solar cells fabricated with **P(T2BDY−TBDT)**, **P(TTzBDY−TBDT)**, **P(T2BDY−TBDT$_{0.7}$−OBDT$_{0.3}$)**, and **P(TTzBDY−TBDT$_{0.7}$−OBDT$_{0.3}$)** donor polymers.

Table 1. Photovoltaic Characteristics of the BODIPY-Based D−A Copolymers

copolymer	V_{oc} [V]	J_{sc} [mA cm^{-2}]	calcd J_{sc}[a] [mA cm^{-2}]	FF	PCE$_{max}$ (PCE$_{avg}$)[b] [%]
P(T2BDY−TBDT)	0.78	12.07	12.53	0.47	4.40 (4.02)
P(TTzBDY−TBDT)	0.80	7.71	7.90	0.40	2.49 (2.37)
P(T2BDY−TBDT$_{0.7}$−OBDT$_{0.3}$)	0.75	3.80	3.84	0.37	1.06 (1.02)
P(TTzBDY−TBDT$_{0.7}$−OBDT$_{0.3}$)	0.77	5.23	5.37	0.39	1.58 (1.51)

[a]Calculated from the integral of the corresponding EQE spectrum. [b]Average value of at least 15 different solar cell devices for each copolymer.

0.0002 ($I_{on}/I_{off} \approx 10^2-10^3$) and 0.0001 cm^2/(V s) ($I_{on}/I_{off} \approx 10^2-10^3$), respectively, whereas the random copolymers **P(T2BDY−TBDT$_{0.7}$−OBDT$_{0.3}$)** and **P(TTzBDY−TBDT$_{0.7}$−OBDT$_{0.3}$)** exhibited relatively lower hole mobilities of ∼3−4 × 10^{-5} cm^2/(V s) ($I_{on}/I_{off} \approx 10^3-10^4$). The observed relatively low charge carrier mobilities for the current copolymers are mainly due to poor thin-film microstructural ordering, which lacks the required in-plane $\pi-\pi$ interactions for charge transport. On the other hand, in addition to their slightly deteriorated surface morphologies, the lower hole mobilities measured for the random copolymers might originate from their lower molecular weights (M_n = 9650 and 10 815 Da vs 29 720 and 30 073 Da) and random π-backbone structures deterring short-range ordering as compared with alternating copolymers.[78] Despite the low LUMOs (from −4.11 to −3.98 eV) measured for the current copolymers, the lack of n-type semiconductivity, even under vacuum, suggests that LUMO π-electron density localization on specific BODIPY units (Figure 4D) impedes electron transport.[79,80] The current copolymers are an excellent example of a π-system in which frontier orbital π-topographies govern charge-transport type rather than the energetics.

Bulk-Heterojunction Solar Cell Devices. The photovoltaic properties and device performances of the four BODIPY-based D−A copolymers **P(T2BDY−TBDT)**, **P(TTzBDY−TBDT)**, **P(T2BDY−TBDT$_{0.7}$−OBDT$_{0.3}$)**, and **P(TTzBDY−TBDT$_{0.7}$−OBDT$_{0.3}$)** were studied in BHJ-OPVs. The solar cells were fabricated in a conventional device architecture of ITO/PEDOT:PSS/active layer/PNDIT-F3N−Br/Ag in which the active layer was fabricated by blending a BODIPY-based D−A copolymer with PC$_{71}$BM acceptor (see the Experimental Section in the Supporting Information for device fabrication details).[81] Relying on the good solubility of the current copolymers, chloroform was employed as the processing solvent and the optimal polymer:fullerene blend weight ratio was determined to be 1:1.8 (w/w) (Table S2). A 1.0 vol % amount of DIO was added into the blend solutions, which optimized the film morphology and enhanced the PCEs of the OPVs (Table S2).[58] All of the BHJ layers were fabricated following the same procedure in order to elucidate the correlation between the BODIPY copolymer structures and the OPV performance.

Figure 6A and 6B shows the current density−voltage (J−V) curves and external quantum efficiency (EQE) responses of the solar cells under AM 1.5G illumination (100 mW cm^{-2}), respectively, and the corresponding photovoltaic parameters (open-circuit voltage (V_{oc}), short-circuit current density (J_{sc}), and fill factor (FF)) are summarized in Table 1. The highest photovoltaic performance was obtained with the **P(T2BDY−TBDT)**-based devices, which showed the maximum PCE of 4.40% with a V_{oc} of 0.78 V, J_{sc} of 12.07 mA cm^{-2}, and FF of 0.47. The **P(TTzBDY−TBDT)**-based devices followed with a PCE value of 2.49% with decreased J_{sc} and FF of 7.71 mA cm^{-2} and 0.40, respectively. Two random copolymers **P(T2BDY−TBDT$_{0.7}$−OBDT$_{0.3}$)** and **P(TTzBDY−TBDT$_{0.7}$−OBDT$_{0.3}$)** exhibited lower PCEs of 1.06 and 1.58%, respectively. To

https://doi.org/10.1021/acsapm.1c01856
ACS Appl. Polym. Mater. 2022, 4, 1991−2005

determine the origin of the superior J_{sc} value observed for **P(T2BDY−TBDT)**-based devices, we compared the hole mobilities of pristine and blend films based on **P(T2BDY−TBDT)** and **P(TTzBDY−TBDT)** via the space-charge-limited current (SCLC) method. As summarized in Table S3, **P(T2BDY−TBDT)** showed better hole-transport ability (μ_h^{SCLC} = 2.59 × 10^{-6} cm^2 V^{-1} s^{-1} for pristine film and 1.29 × 10^{-6} cm^2 V^{-1} s^{-1} for blend film) than **P(TTzBDY−TBDT)** (μ_h^{SCLC} = 6.54 × 10^{-7} cm^2 V^{-1} s^{-1} for pristine film and 7.54 × 10^{-7} cm^2 V^{-1} s^{-1} for blend film). The calculated J_{sc} values from the EQE spectra of all devices (Figure 6B) agreed well with the corresponding measured J_{sc} values from the $J-V$ curves (Figure 6A) within an error of ∼5%. Comparing the electrochemical properties of the donor polymers with the solar cell device characteristics, the V_{oc} and the HOMO energy level trends were generally consistent.

To better understand the exciton dissociation and recombination properties of the blend films that are deeply associated with the J_{sc} and FF trends, exciton dissociation probabilities ($P(E,T)$s) and light intensity (P)-dependent V_{oc} measurements were performed (Figure 6C and 6D). The $P(E,T)$ for each device was obtained from the ratio between the photocurrent density (J_{ph}) at short-circuit condition and the saturated J_{ph} value, where the effective voltage (V_{eff}) is 3 V.[82] Consistent with the photovoltaic performance trends, alternating copolymers **P(T2BDY−TBDT)** and **P(TTzBDY−TBDT)** showed higher $P(E,T)$ values of 79.0% and 62.1%, respectively, when compared with those of the random copolymers ($P(E,T)$ = 48.0−54.5%). Furthermore, the relationships of V_{oc} vs ln(P_{light}) from 0.1 to 1 Sun are shown in Figure 6D for all copolymers, including the slopes (S) with units of k_BTq^{-1}, where k_B is the Boltzmann constant, T is the temperature, and q is the elementary charge.[83] The **P(T2BDY−TBDT)**-based blend showed the smallest S value of 1.36, while the other copolymers exhibited similar S values of 1.45−1.48, which suggests that monomolecular recombination was most suppressed in **P(T2BDY−TBDT):$PC_{71}BM$** blend. The series of superior photophysical properties observed for **P(T2BDY−TBDT)** explain the origin of the highest FF value among the current copolymers. Lastly, the surface morphologies of the current polymer:fullerene blend films were studied by AFM and optical microscopy (OM). During the device fabrication process, we found that the solubility of the blend solutions based on (**P(T2BDY−TBDT)** and **P(TTzBDY−TBDT)**) was slightly better than that of **P(T2BDY−$TBDT_{0.7}$−$OBDT_{0.3}$)** and **P(TTzBDY−$TBDT_{0.7}$−$OBDT_{0.3}$)**. As shown in Figure S33, the blend films based on **P(T2BDY−TBDT)** and **P(TTzBDY−TBDT)** yielded relatively smooth surfaces with a low rms roughness of ∼0.5−0.6 nm. However, the random copolymers were found to form relatively large aggregates, which might limit the charge transport and exciton dissociation properties and decrease the J_{sc} and FF values. The relatively low PCEs for the current BODIPY-based solar cells are mainly due to the reduced light absorption from the use of the fullerene acceptor and the low FFs. The J_{sc} value could be enhanced by pairing our polymer donors with nonfullerene small molecule or polymer acceptors that strongly absorb light in the visible and infrared range. On the other hand, optimizing the blend morphology by controlling the solvent type, using additives, and thermal annealing could be an important direction to improve the FF.

CONCLUSION

In summary, we demonstrated the theory-aided rational design, challenging synthesis, and full characterization of meso-π-extended/deficient BODIPY building blocks, **2OD−T2BDY** and **2OD−TTzBDY**, for use in the development of low-band-gap D−A copolymers. The building blocks showed favorable π-acceptor electronic/structural properties with meso-π-delocalized and stabilized LUMOs (∼−3.6 eV) and large ground-state dipole moments of 4.9−5.5 D. These building blocks, to the best of our knowledge, are the first examples of BODIPYs with meso-π-extension in the optoelectronics literature. Meso-π-extension was also found to be effective in terms of extending the optical absorption in the visible region via the contribution of HOMO−1 orbitals. A copolymerization screening strategy with three different relatively π-electron-rich comonomers was employed to yield eight different copolymers, four of which have sufficient solubilities in common organic solvents. The copolymers **P(T2BDY−TBDT)**, **P(TTzBDY−TBDT)**, **P(T2BDY−$TBDT_{0.7}$−$OBDT_{0.3}$)**, and **P(TTzBDY−$TBDT_{0.7}$−$OBDT_{0.3}$)** showed HOMO energies from −5.3 to −5.4 eV and LUMO energies from −4.0 to −4.1 eV, yielding optical band gaps of 1.30−1.35 eV. Consistent with the theoretical/experimental π-electronic structures of the current polymer backbones, all copolymers functioned as p-type semiconductors in BG−TC OFETs and as donor materials with the $PC_{71}BM$ acceptor in the BHJ-OPVs. PCEs of up to 4.4% with J_{sc}'s of up to 12.07 mA cm^{-2} were achieved. Our findings revealed that meso-π-extension is an effective strategy to realize BODIPYs with favorable π-acceptor properties. The BODIPYs developed herein contribute to the structural diversity of not only BODIPY-based structures but also π-acceptors in the optoelectronics literature and could open up future materials design avenues in varied organic optoelectronic applications. Different (hetero)aryl units (e.g., pyridine, pyrimidine) or longer meso-π-extensions (e.g., three or more units) could be employed in future research to further explore this strategy.

ASSOCIATED CONTENT

Supporting Information

The Supporting Information is available free of charge at https://pubs.acs.org/doi/10.1021/acsapm.1c01856.

Chemical structures and BHJ-OPV characteristics of previously reported BODIPY-based D−A polymers; experimental methods and equipment; BHJ-OPV and OFET fabrication methods; syntheses of 2-octyl-1-bromododecane and 2-methylpyrrole and chemical characterization; syntheses and $^1H/^{13}C$ NMR and MALDI TOF/APCI-MS spectra for **1−5**, **2OD−T2-COH**, **2OD−T2BDY**, **2OD−TTz-COH**, **2OD−T2BDY−Br_2**, and **2OD−TTzBDY−Br_2**; syntheses and ^1H NMR spectra of **2OD−T-COH** and **2OD−TBDY**; full-range cyclic voltammograms of **2OD−T2BDY** and **2OD−TTzBDY**; synthesis and ^1H NMR spectra for polymers; thermogravimetric analysis curves, solvent/temperature-dependent/solid-state optical absorption spectra, HOMO−LUMO frontier orbital energy saturation, and topographies/energies for the tetramer models of **P(T2BDY−TBDT)**, **P(TTzBDY−TBDT)**, **P(T2BDY−$TBDT_{0.7}$−$OBDT_{0.3}$)**, and **P(TTzBDY−$TBDT_{0.7}$−$OBDT_{0.3}$)**; AFM and OM images of the

https://doi.org/10.1021/acsapm.1c01856
ACS Appl. Polym. Mater. 2022, 4, 1991−2005

BODIPY-based Polymer:$PC_{71}BM$ blend films; photovoltaic performance values and SCLC mobilities (PDF)

AUTHOR INFORMATION

Corresponding Authors

Choongik Kim − *Department of Chemical and Biomolecular Engineering, Sogang University, Mapo-gu, Seoul 04107, Republic of Korea;* orcid.org/0000-0001-7494-0677; Email: choongik@sogang.ac.kr

Bumjoon J. Kim − *Department of Chemical and Biomolecular Engineering, Korea Advanced Institute of Science and Technology (KAIST), Daejeon 34141, Republic of Korea;* orcid.org/0000-0001-7783-9689; Email: bjkim02@kaist.ac.kr

Hakan Usta − *Department of Nanotechnology Engineering, Abdullah Gül University, Kayseri 38080, Turkey;* orcid.org/0000-0002-0618-1979; Email: hakan.usta@agu.edu.tr

Authors

Ayse Can − *Department of Nanotechnology Engineering, Abdullah Gül University, Kayseri 38080, Turkey*

Gi-Seok Choi − *Department of Chemical and Biomolecular Engineering, Korea Advanced Institute of Science and Technology (KAIST), Daejeon 34141, Republic of Korea*

Resul Ozdemir − *Department of Nanotechnology Engineering, Abdullah Gül University, Kayseri 38080, Turkey;* orcid.org/0000-0002-7957-110X

Soyoon Park − *Department of Chemical and Biomolecular Engineering, Sogang University, Mapo-gu, Seoul 04107, Republic of Korea*

Jin Su Park − *Department of Chemical and Biomolecular Engineering, Korea Advanced Institute of Science and Technology (KAIST), Daejeon 34141, Republic of Korea*

Yongchul Lee − *Department of Chemical and Biomolecular Engineering, Sogang University, Mapo-gu, Seoul 04107, Republic of Korea*

İbrahim Deneme − *Department of Nanotechnology Engineering, Abdullah Gül University, Kayseri 38080, Turkey*

Evren Mutlugun − *Department of Electrical and Electronics Engineering, Abdullah Gül University, Kayseri 38080, Turkey;* orcid.org/0000-0003-3715-5594

Complete contact information is available at: https://pubs.acs.org/10.1021/acsapm.1c01856

Notes

The authors declare no competing financial interest.

ACKNOWLEDGMENTS

H.U., E.M., A.C., R.O., and İ.D. acknowledge support from the Scientific and Technological Research Council of Turkey (TUBITAK) (grant no. 119F153). We thank Prof. Bunyemin Cosut for his help with the quantum efficiency/decay measurements.

REFERENCES

(1) Hwang, I.-W.; Moses, D.; Heeger, A. J. Photoinduced Carrier Generation in P3HT/PCBM Bulk Heterojunction Materials. *J. Phys. Chem. C* **2008**, *112* (11), 4350−4354.

(2) Cui, Y.; Yao, H.; Hong, L.; Zhang, T.; Xu, Y.; Xian, K.; Gao, B.; Qin, J.; Zhang, J.; Wei, Z.; Hou, J. Achieving Over 15% Efficiency in Organic Photovoltaic Cells via Copolymer Design. *Adv. Mater.* **2019**, *31* (14), 1808356.

(3) Gao, W.; Zhang, M.; Liu, T.; Ming, R.; An, Q.; Wu, K.; Xie, D.; Luo, Z.; Zhong, C.; Liu, F.; Zhang, F.; Yan, H.; Yang, C. Asymmetrical Ladder-Type Donor-Induced Polar Small Molecule Acceptor to Promote Fill Factors Approaching 77% for High-Performance Nonfullerene Polymer Solar Cells. *Adv. Mater.* **2018**, *30* (26), 1800052.

(4) Cui, Y.; Yao, H.; Zhang, J.; Zhang, T.; Wang, Y.; Hong, L.; Xian, K.; Xu, B.; Zhang, S.; Peng, J.; Wei, Z.; Gao, F.; Hou, J. Over 16% Efficiency Organic Photovoltaic Cells Enabled by a Chlorinated Acceptor with Increased Open-Circuit Voltages. *Nat. Commun.* **2019**, *10* (1), 2515.

(5) Li, S.; Li, C.-Z.; Shi, M.; Chen, H. New Phase for Organic Solar Cell Research: Emergence of Y-Series Electron Acceptors and Their Perspectives. *ACS Energy Lett.* **2020**, *5* (5), 1554−1567.

(6) Kim, T.; Kim, J.-H.; Kang, T. E.; Lee, C.; Kang, H.; Shin, M.; Wang, C.; Ma, B.; Jeong, U.; Kim, T.-S.; Kim, B. J. Flexible, Highly Efficient All-Polymer Solar Cells. *Nat. Commun.* **2015**, *6* (1), 8547.

(7) Schroeder, B. C.; Chiu, Y.; Gu, X.; Zhou, Y.; Xu, J.; Lopez, J.; Lu, C.; Toney, M. F.; Bao, Z. Non-Conjugated Flexible Linkers in Semiconducting Polymers: A Pathway to Improved Processability without Compromising Device Performance. *Adv. Electron. Mater.* **2016**, *2* (7), 1600104.

(8) Balar, N.; Xiong, Y.; Ye, L.; Li, S.; Nevola, D.; Dougherty, D. B.; Hou, J.; Ade, H.; O'Connor, B. T. Role of Polymer Segregation on the Mechanical Behavior of All-Polymer Solar Cell Active Layers. *ACS Appl. Mater. Interfaces* **2017**, *9* (50), 43886−43892.

(9) Choi, J.; Kim, W.; Kim, D.; Kim, S.; Chae, J.; Choi, S. Q.; Kim, F. S.; Kim, T.-S.; Kim, B. J. Importance of Critical Molecular Weight of Semicrystalline N-Type Polymers for Mechanically Robust, Efficient Electroactive Thin Films. *Chem. Mater.* **2019**, *31* (9), 3163−3173.

(10) Jindal, A.; Kotani, H.; Kushida, S.; Saeki, A.; Kojima, T.; Yamamoto, Y. Significant Enhancement of Hole Transport Ability in Conjugated Polymer/Fullerene Bulk Heterojunction Microspheres. *ACS Appl. Polym. Mater.* **2019**, *1* (2), 118−123.

(11) Facchetti, A. Polymer Donor−Polymer Acceptor (All-Polymer) Solar Cells. *Mater. Today* **2013**, *16* (4), 123−132.

(12) Lee, C.; Lee, S.; Kim, G.-U.; Lee, W.; Kim, B. J. Recent Advances, Design Guidelines, and Prospects of All-Polymer Solar Cells. *Chem. Rev.* **2019**, *119* (13), 8028−8086.

(13) Cui, C.; Li, Y. High-Performance Conjugated Polymer Donor Materials for Polymer Solar Cells with Narrow-Bandgap Nonfullerene Acceptors. *Energy Environ. Sci.* **2019**, *12* (11), 3225−3246.

(14) Sun, H.; Yu, H.; Shi, Y.; Yu, J.; Peng, Z.; Zhang, X.; Liu, B.; Wang, J.; Singh, R.; Lee, J.; Li, Y.; Wei, Z.; Liao, Q.; Kan, Z.; Ye, L.; Yan, H.; Gao, F.; Guo, X. A Narrow-Bandgap N-Type Polymer with an Acceptor−Acceptor Backbone Enabling Efficient All-Polymer Solar Cells. *Adv. Mater.* **2020**, *32* (43), 2004183.

(15) Zhan, X.; Zhu, D. Conjugated Polymers for High-Efficiency Organic Photovoltaics. *Polym. Chem.* **2010**, *1* (4), 409−419.

(16) Lobez, J. M.; Andrew, T. L.; Bulović, V.; Swager, T. M. Improving the Performance of P3HT−Fullerene Solar Cells with Side-Chain-Functionalized Poly(Thiophene) Additives: A New Paradigm for Polymer Design. *ACS Nano* **2012**, *6* (4), 3044−3056.

(17) Li, G.; Shrotriya, V.; Huang, J.; Yao, Y.; Moriarty, T.; Emery, K.; Yang, Y. High-Efficiency Solution Processable Polymer Photovoltaic Cells by Self-Organization of Polymer Blends. *Nat. Mater.* **2005**, *4* (11), 864−868.

(18) Nguyen, L. H.; Hoppe, H.; Erb, T.; Günes, S.; Gobsch, G.; Sariciftci, N. S. Effects of Annealing on the Nanomorphology and Performance of Poly(Alkylthiophene):Fullerene Bulk-Heterojunction Solar Cells. *Adv. Funct. Mater.* **2007**, *17* (7), 1071−1078.

(19) Halls, J. J. M.; Walsh, C. A.; Greenham, N. C.; Marseglia, E. A.; Friend, R. H.; Moratti, S. C.; Holmes, A. B. Efficient Photodiodes from Interpenetrating Polymer Networks. *Nature* **1995**, *376* (6540), 498−500.

(20) Tajima, K.; Suzuki, Y.; Hashimoto, K. Polymer Photovoltaic Devices Using Fully Regioregular Poly[(2-Methoxy-5-(3′,7′-Dime-

thyloctyloxy))-1,4-Phenylenevinylene]. *J. Phys. Chem. C* **2008**, *112* (23), 8507−8510.
(21) Lu, L.; Zheng, T.; Wu, Q.; Schneider, A. M.; Zhao, D.; Yu, L. Recent Advances in Bulk Heterojunction Polymer Solar Cells. *Chem. Rev.* **2015**, *115* (23), 12666−12731.
(22) Jung, H.; Jung, A.-R.; Jin, S.-M.; Kim, S.; Heo, H.; Nguyen, H. V. T.; Kim, M. J.; Ahn, P.; Kim, M. H.; Lee, Y.; Lee, K.-K.; Cho, J. H.; Lee, E.; Kim, B. Influence of 3D Morphology on the Performance of All-Polymer Solar Cells Processed Using Environmentally Benign Nonhalogenated Solvents. *Nano Energy* **2020**, *77*, 105106.
(23) Zhang, G.; Ning, H.; Chen, H.; Jiang, Q.; Jiang, J.; Han, P.; Dang, L.; Xu, M.; Shao, M.; He, F.; Wu, Q. Naphthalenothiophene Imide-Based Polymer Exhibiting over 17% Efficiency. *Joule* **2021**, *5* (4), 931−944.
(24) Lee, J.-W.; Jeong, D.; Kim, D. J.; Phan, T. N.-L.; Park, J. S.; Kim, T.-S.; Kim, B. J. Flexible-Spacer Incorporated Polymer Donors Enable Superior Blend Miscibility for High-Performance and Mechanically-Robust Polymer Solar Cells. *Energy Environ. Sci.* **2021**, *14* (7), 4067−4076.
(25) Cui, Y.; Yao, H.; Zhang, J.; Xian, K.; Zhang, T.; Hong, L.; Wang, Y.; Xu, Y.; Ma, K.; An, C.; He, C.; Wei, Z.; Gao, F.; Hou, J. Single-Junction Organic Photovoltaic Cells with Approaching 18% Efficiency. *Adv. Mater.* **2020**, *32* (19), 1908205.
(26) Liang, Y.; Xiao, S.; Feng, D.; Yu, L. Control in Energy Levels of Conjugated Polymers for Photovoltaic Application. *J. Phys. Chem. C* **2008**, *112* (21), 7866−7871.
(27) Qu, S.; Tian, H. Diketopyrrolopyrrole (DPP)-Based Materials for Organic Photovoltaics. *Chem. Commun.* **2012**, *48* (25), 3039−3051.
(28) Lu, S.; Drees, M.; Yao, Y.; Boudinet, D.; Yan, H.; Pan, H.; Wang, J.; Li, Y.; Usta, H.; Facchetti, A. 3,6-Dithiophen-2-Yl-Diketopyrrolo[3,2- b]Pyrrole (IsoDPPT) as an Acceptor Building Block for Organic Opto-Electronics. *Macromolecules* **2013**, *46* (10), 3895−3906.
(29) Zhang, H.; Yao, H.; Hou, J.; Zhu, J.; Zhang, J.; Li, W.; Yu, R.; Gao, B.; Zhang, S.; Hou, J. Over 14% Efficiency in Organic Solar Cells Enabled by Chlorinated Nonfullerene Small-Molecule Acceptors. *Adv. Mater.* **2018**, *30* (28), 1800613.
(30) Zheng, B.; Huo, L.; Li, Y. Benzodithiophenedione-Based Polymers: Recent Advances in Organic Photovoltaics. *NPG Asia Mater.* **2020**, *12* (1), 3.
(31) Zhou, J.; Cong, P.; Chen, L.; Zhang, B.; Geng, Y.; Tang, A.; Zhou, E. Gradually Modulating the Three Parts of D-π-A Type Polymers for High-Performance Organic Solar Cells. *J. Energy Chem.* **2021**, *62*, 532−537.
(32) Tang, A.; Zhang, Q.; Du, M.; Li, G.; Geng, Y.; Zhang, J.; Wei, Z.; Sun, X.; Zhou, E. Molecular Engineering of D−π−A Copolymers Based on 4,8-Bis(4-Chlorothiophen-2-Yl)Benzo[1,2- b:4,5-b ′]-Dithiophene (BDT-T-Cl) for High-Performance Fullerene-Free Organic Solar Cells. *Macromolecules* **2019**, *52* (16), 6227−6233.
(33) Park, J. S.; Kim, G.-U.; Lee, D.; Lee, S.; Ma, B.; Cho, S.; Kim, B. J. Importance of Optimal Crystallinity and Hole Mobility of BDT-Based Polymer Donor for Simultaneous Enhancements of V_{oc}, J_{sc}, and FF in Efficient Nonfullerene Organic Solar Cells. *Adv. Funct. Mater.* **2020**, *30* (51), 2005787.
(34) Guo, X.; Xin, H.; Kim, F. S.; Liyanage, A. D. T.; Jenekhe, S. A.; Watson, M. D. Thieno[3,4-c]Pyrrole-4,6-Dione-Based Donor−Acceptor Conjugated Polymers for Solar Cells. *Macromolecules* **2011**, *44* (2), 269−277.
(35) Wu, J.; Li, G.; Fang, J.; Guo, X.; Zhu, L.; Guo, B.; Wang, Y.; Zhang, G.; Arunagiri, L.; Liu, F.; Yan, H.; Zhang, M.; Li, Y. Random Terpolymer Based on Thiophene-Thiazolothiazole Unit Enabling Efficient Non-Fullerene Organic Solar Cells. *Nat. Commun.* **2020**, *11* (1), 4612.
(36) Lee, J.-W.; Choi, N.; Kim, D.; Phan, T. N.-L.; Kang, H.; Kim, T.-S.; Kim, B. J. Side Chain Engineered Naphthalene Diimide-Based Terpolymer for Efficient and Mechanically Robust All-Polymer Solar Cells. *Chem. Mater.* **2021**, *33* (3), 1070−1081.
(37) Yao, H.; Bai, F.; Hu, H.; Arunagiri, L.; Zhang, J.; Chen, Y.; Yu, H.; Chen, S.; Liu, T.; Lai, J. Y. L.; Zou, Y.; Ade, H.; Yan, H. Efficient All-Polymer Solar Cells Based on a New Polymer Acceptor Achieving 10.3% Power Conversion Efficiency. *ACS Energy Lett.* **2019**, *4* (2), 417−422.
(38) Yang, J.; An, N.; Sun, S.; Sun, X.; Nakano, M.; Takimiya, K.; Xiao, B.; Zhou, E. The Effect of Alkyl Chain Branching Positions on the Electron Mobility and Photovoltaic Performance of Naphthodithiophene Diimide (NDTI)-Based Polymers. *Sci. China Chem.* **2019**, *62* (12), 1649−1655.
(39) Lin, Y.-C.; Chen, C.-H.; Li, R.-H.; Tsao, C.-S.; Saeki, A.; Wang, H.-C.; Chang, B.; Huang, L.-Y.; Yang, Y.; Wei, K.-H. Atom-Varied Side Chains in Conjugated Polymers Affect Efficiencies of Photovoltaic Devices Incorporating Small Molecules. *ACS Appl. Polym. Mater.* **2020**, *2* (2), 636−646.
(40) Raju, T. B.; Cho, H. W.; Gopikrishna, P.; Lee, Y.; Kim, J. Y.; Kim, B. Positional Effect of the 2-Ethylhexyl Carboxylate Side Chain on the Thiophene π-Bridge of Nonfullerene Acceptors for Efficient Organic Solar Cells. *ACS Appl. Energy Mater.* **2021**, *4* (10), 11675−11683.
(41) Zhang, J.; Tan, H. S.; Guo, X.; Facchetti, A.; Yan, H. Material Insights and Challenges for Non-Fullerene Organic Solar Cells Based on Small Molecular Acceptors. *Nat. Energy* **2018**, *3* (9), 720−731.
(42) Li, W.; Ye, L.; Li, S.; Yao, H.; Ade, H.; Hou, J. A High-Efficiency Organic Solar Cell Enabled by the Strong Intramolecular Electron Push−Pull Effect of the Nonfullerene Acceptor. *Adv. Mater.* **2018**, *30* (16), 1707170.
(43) Liu, W.; Xu, X.; Yuan, J.; Leclerc, M.; Zou, Y.; Li, Y. Low-Bandgap Non-Fullerene Acceptors Enabling High-Performance Organic Solar Cells. *ACS Energy Lett.* **2021**, *6* (2), 598−608.
(44) Chao, P.; Chen, H.; Zhu, Y.; Lai, H.; Mo, D.; Zheng, N.; Chang, X.; Meng, H.; He, F. A Benzo[1,2-b:4,5-c′]Dithiophene-4,8-Dione-Based Polymer Donor Achieving an Efficiency Over 16%. *Adv. Mater.* **2020**, *32* (10), 1907059.
(45) Lin, F.; Jiang, K.; Kaminsky, W.; Zhu, Z.; Jen, A. K. Y. A Non-Fullerene Acceptor with Enhanced Intermolecular π-Core Interaction for High-Performance Organic Solar Cells. *J. Am. Chem. Soc.* **2020**, *142* (36), 15246−15251.
(46) Lee, J.; Sun, C.; Ma, B. S.; Kim, H. J.; Wang, C.; Ryu, J. M.; Lim, C.; Kim, T.; Kim, Y.; Kwon, S.; Kim, B. J. Efficient, Thermally Stable, and Mechanically Robust All-Polymer Solar Cells Consisting of the Same Benzodithiophene Unit-Based Polymer Acceptor and Donor with High Molecular Compatibility. *Adv. Energy Mater.* **2021**, *11* (5), 2003367.
(47) Fan, Q.; Su, W.; Chen, S.; Kim, W.; Chen, X.; Lee, B.; Liu, T.; Méndez-Romero, U. A.; Ma, R.; Yang, T.; Zhuang, W.; Li, Y.; Li, Y.; Kim, T.-S.; Hou, L.; Yang, C.; Yan, H.; Yu, D.; Wang, E. Mechanically Robust All-Polymer Solar Cells from Narrow Band Gap Acceptors with Hetero-Bridging Atoms. *Joule* **2020**, *4* (3), 658−672.
(48) Ren, H.; Chen, J.; Li, Y.; Tang, J. Recent Progress in Organic Photodetectors and Their Applications. *Adv. Sci.* **2021**, *8* (1), 2002418.
(49) Gibert-Roca, M.; Molet, P.; Mihi, A.; Campoy-Quiles, M. Near Infrared Organic Photodetectors Based on Enhanced Charge Transfer State Absorption by Photonic Architectures. *J. Mater. Chem. C* **2020**, *8* (28), 9688−9696.
(50) Vegiraju, S.; Lin, C.-Y.; Priyanka, P.; Huang, D.-Y.; Luo, X.-L.; Tsai, H.-C.; Hong, S.-H.; Yeh, C.-J.; Lien, W.-C.; Wang, C.-L.; Tung, S.-H.; Liu, C.-L.; Chen, M.-C.; Facchetti, A. Solution-Processed High-Performance Tetrathienothiophene-Based Small Molecular Blends for Ambipolar Charge Transport. *Adv. Funct. Mater.* **2018**, *28* (28), 1801025.
(51) Vegiraju, S.; Luo, X.-L.; Li, L.-H.; Afraj, S. N.; Lee, C.; Zheng, D.; Hsieh, H.-C.; Lin, C.-C.; Hong, S.-H.; Tsai, H.-C.; Lee, G.-H.; Tung, S.-H.; Liu, C.-L.; Chen, M.-C.; Facchetti, A. Solution Processable Pseudo n -Thienoacenes via Intramolecular S···S Lock for High Performance Organic Field Effect Transistors. *Chem. Mater.* **2020**, *32* (4), 1422−1429.

https://doi.org/10.1021/acsapm.1c01856
ACS Appl. Polym. Mater. 2022, 4, 1991−2005

(52) Yu, Z.-P.; Yan, K.; Ullah, W.; Chen, H.; Li, C.-Z. Conjugated Polymers for Photon-to-Electron and Photon-to-Fuel Conversions. *ACS Appl. Polym. Mater.* **2021**, *3* (1), 60−92.
(53) Holt, E. D.; Wang, J.; Winkel, R. W.; Younus, M.; Schanze, K. S. Photophysics and Solar Cell Application of a Benzodithiophene Conjugated Polymer Containing Cyclometalated Platinum Units. *J. Photochem. Photobiol.* **2021**, *8*, 100060.
(54) Nhon, L.; Taggart, A. D.; Moot, T.; Brennaman, M. K.; Jagadesan, P.; Schanze, K. S.; Cahoon, J. F.; Reynolds, J. R. Organic Chromophores Designed for Hole Injection into Wide-Band-Gap Metal Oxides for Solar Fuel Applications. *Chem. Mater.* **2020**, *32* (19), 8158−8168.
(55) Ozcan, E.; Ozdemir, M.; Ho, D.; Zorlu, Y.; Ozdemir, R.; Kim, C.; Usta, H.; Cosut, B. A Solution-Processable Meso-Phenyl-BODIPY-Based N-Channel Semiconductor with Enhanced Fluorescence Emission. *ChemPlusChem.* **2019**, *84* (9), 1423−1431.
(56) Squeo, B. M.; Gasparini, N.; Ameri, T.; Palma-Cando, A.; Allard, S.; Gregoriou, V. G.; Brabec, C. J.; Scherf, U.; Chochos, C. L. Ultra Low Band Gap α,β-Unsubstituted BODIPY-Based Copolymer Synthesized by Palladium Catalyzed Cross-Coupling Polymerization for near Infrared Organic Photovoltaics. *J. Mater. Chem. A* **2015**, *3* (31), 16279−16286.
(57) Kim, B.; Ma, B.; Donuru, V. R.; Liu, H.; Fréchet, J. M. J. Bodipy-Backboned Polymers as Electron Donor in Bulk Heterojunction Solar Cells. *Chem. Commun.* **2010**, *46* (23), 4148.
(58) Ozdemir, M.; Kim, S. W.; Kim, H.; Kim, M.-G.; Kim, B. J.; Kim, C.; Usta, H. Semiconducting Copolymers Based on Meso -Substituted BODIPY for Inverted Organic Solar Cells and Field-Effect Transistors. *Adv. Electron. Mater.* **2018**, *4* (10), 1700354.
(59) Liu, B.; Ma, Z.; Xu, Y.; Guo, Y.; Yang, F.; Xia, D.; Li, C.; Tang, Z.; Li, W. Non-Fullerene Organic Solar Cells Based on a BODIPY-Polymer as Electron Donor with High Photocurrent. *J. Mater. Chem. C* **2020**, *8* (7), 2232−2237.
(60) Bucher, L.; Desbois, N.; Harvey, P. D.; Gros, C. P.; Misra, R.; Sharma, G. D. Nonfullerene Polymer Solar Cells Reaching a 9.29% Efficiency Using a BODIPY-Thiophene Backboned Donor Material. *ACS Appl. Energy Mater.* **2018**, *1* (7), 3359−3368.
(61) Ozdemir, M.; Choi, D.; Kwon, G.; Zorlu, Y.; Cosut, B.; Kim, H.; Facchetti, A.; Kim, C.; Usta, H. Solution-Processable BODIPY-Based Small Molecules for Semiconducting Microfibers in Organic Thin-Film Transistors. *ACS Appl. Mater. Interfaces* **2016**, *8* (22), 14077−14087.
(62) Usta, H.; Sheets, W. C.; Denti, M.; Generali, G.; Capelli, R.; Lu, S.; Yu, X.; Muccini, M.; Facchetti, A. Perfluoroalkyl-Functionalized Thiazole−Thiophene Oligomers as N-Channel Semiconductors in Organic Field-Effect and Light-Emitting Transistors. *Chem. Mater.* **2014**, *26* (22), 6542−6556.
(63) Zaborova, E.; Chávez, P.; Bechara, R.; Lévêque, P.; Heiser, T.; Méry, S.; Leclerc, N. Thiazole as a Weak Electron-Donor Unit to Lower the Frontier Orbital Energy Levels of Donor−Acceptor Alternating Conjugated Materials. *Chem. Commun.* **2013**, *49* (85), 9938−9940.
(64) Su, H.-L.; Sredojevic, D. N.; Bronstein, H.; Marks, T. J.; Schroeder, B. C.; Al-Hashimi, M. Bithiazole: An Intriguing Electron-Deficient Building for Plastic Electronic Applications. *Macromol. Rapid Commun.* **2017**, *38* (10), 1600610.
(65) Ozdemir, M.; Choi, D.; Zorlu, Y.; Cosut, B.; Kim, H.; Kim, C.; Usta, H. A New Rod-Shaped BODIPY-Acetylene Molecule for Solution-Processed Semiconducting Microribbons in n-Channel Organic Field-Effect Transistors. *New J. Chem.* **2017**, *41* (14), 6232−6240.
(66) Naraso; Wudl, F. Two Poly(2,5-Thienythiazolothiazole)s: Observation of Spontaneous Ordering in Thin Films. *Macromolecules* **2008**, *41* (9), 3169−3174.
(67) Bronstein, H.; Hurhangee, M.; Fregoso, E. C.; Beatrup, D.; Soon, Y. W.; Huang, Z.; Hadipour, A.; Tuladhar, P. S.; Rossbauer, S.; Sohn, E.-H.; Shoaee, S.; Dimitrov, S. D.; Frost, J. M.; Ashraf, R. S.; Kirchartz, T.; Watkins, S. E.; Song, K.; Anthopoulos, T.; Nelson, J.; Rand, B. P.; Durrant, J. R.; McCulloch, I. Isostructural, Deeper Highest Occupied Molecular Orbital Analogues of Poly(3-Hexylthiophene) for High-Open Circuit Voltage Organic Solar Cells. *Chem. Mater.* **2013**, *25* (21), 4239−4249.
(68) Letizia, J. A.; Salata, M. R.; Tribout, C. M.; Facchetti, A.; Ratner, M. A.; Marks, T. J. N-Channel Polymers by Design: Optimizing the Interplay of Solubilizing Substituents, Crystal Packing, and Field-Effect Transistor Characteristics in Polymeric Bithiophene-Imide Semiconductors. *J. Am. Chem. Soc.* **2008**, *130* (30), 9679−9694.
(69) Carsten, B.; Szarko, J. M.; Son, H. J.; Wang, W.; Lu, L.; He, F.; Rolczynski, B. S.; Lou, S. J.; Chen, L. X.; Yu, L. Examining the Effect of the Dipole Moment on Charge Separation in Donor−Acceptor Polymers for Organic Photovoltaic Applications. *J. Am. Chem. Soc.* **2011**, *133* (50), 20468−20475.
(70) Usta, H.; Yilmaz, M. D.; Avestro, A.-J.; Boudinet, D.; Denti, M.; Zhao, W.; Stoddart, J. F.; Facchetti, A. BODIPY-Thiophene Copolymers as p -Channel Semiconductors for Organic Thin-Film Transistors. *Adv. Mater.* **2013**, *25* (31), 4327−4334.
(71) Carsten, B.; Szarko, J. M.; Lu, L.; Son, H. J.; He, F.; Botros, Y. Y.; Chen, L. X.; Yu, L. Mediating Solar Cell Performance by Controlling the Internal Dipole Change in Organic Photovoltaic Polymers. *Macromolecules* **2012**, *45* (16), 6390−6395.
(72) Lei, T.; Dou, J.-H.; Pei, J. Influence of Alkyl Chain Branching Positions on the Hole Mobilities of Polymer Thin-Film Transistors. *Adv. Mater.* **2012**, *24* (48), 6457−6461.
(73) Stangeland, E. L.; Sammakia, T. Use of Thiazoles in the Halogen Dance Reaction: Application to the Total Synthesis of WS75624 B. *J. Org. Chem.* **2004**, *69* (7), 2381−2385.
(74) Cho, D. W.; Fujitsuka, M.; Ryu, J. H.; Lee, M. H.; Kim, H. K.; Majima, T.; Im, C. S2 Emission from Chemically Modified BODIPYs. *Chem. Commun.* **2012**, *48* (28), 3424.
(75) Kim, S. W.; Choi, J.; Bui, T. T. T.; Lee, C.; Cho, C.; Na, K.; Jung, J.; Song, C. E.; Ma, B.; Lee, J.-Y.; Shin, W. S.; Kim, B. J. Rationally Designed Donor-Acceptor Random Copolymers with Optimized Complementary Light Absorption for Highly Efficient All-Polymer Solar Cells. *Adv. Funct. Mater.* **2017**, *27* (38), 1703070.
(76) Park, S. H.; Lee, H. S.; Kim, J.-D.; Breiby, D. W.; Kim, E.; Park, Y. D.; Ryu, D. Y.; Lee, D. R.; Cho, J. H. A Polymer Brush Organic Interlayer Improves the Overlying Pentacene Nanostructure and Organic Field-Effect Transistor Performance. *J. Mater. Chem.* **2011**, *21* (39), 15580−15586.
(77) Hwang, D.-H.; Nomura, A.; Kim, J.; Kim, J.-H.; Cho, H.; Lee, C.; Ohno, K.; Tsujii, Y. Synthesis and Characterization of Polystyrene Brushes for Organic Thin Film Transistors. *J. Nanosci. Nanotechnol.* **2012**, *12* (5), 4137−4141.
(78) Kline, R. J.; McGehee, M. D.; Kadnikova, E. N.; Liu, J.; Fréchet, J. M. J.; Toney, M. F. Dependence of Regioregular Poly(3-Hexylthiophene) Film Morphology and Field-Effect Mobility on Molecular Weight. *Macromolecules* **2005**, *38* (8), 3312−3319.
(79) Ryu, G.-S.; Chen, Z.; Usta, H.; Noh, Y.-Y.; Facchetti, A. Naphthalene Diimide-Based Polymeric Semiconductors. Effect of Chlorine Incorporation and n-Channel Transistors Operating in Water. *MRS Commun.* **2016**, *6* (1), 47−60.
(80) Figà, V.; Chiappara, C.; Ferrante, F.; Casaletto, M. P.; Principato, F.; Cataldo, S.; Chen, Z.; Usta, H.; Facchetti, A.; Pignataro, B. Symmetric Naphthalenediimidequaterthiophenes for Electropolymerized Electrochromic Thin Films. *J. Mater. Chem. C* **2015**, *3* (23), 5985−5994.
(81) Wu, Z.; Sun, C.; Dong, S.; Jiang, X.-F.; Wu, S.; Wu, H.; Yip, H.-L.; Huang, F.; Cao, Y. N-Type Water/Alcohol-Soluble Naphthalene Diimide-Based Conjugated Polymers for High-Performance Polymer Solar Cells. *J. Am. Chem. Soc.* **2016**, *138* (6), 2004−2013.
(82) Chen, W.; Xu, T.; He, F.; Wang, W.; Wang, C.; Strzalka, J.; Liu, Y.; Wen, J.; Miller, D. J.; Chen, J.; Hong, K.; Yu, L.; Darling, S. B. Hierarchical Nanomorphologies Promote Exciton Dissociation in Polymer/Fullerene Bulk Heterojunction Solar Cells. *Nano Lett.* **2011**, *11* (9), 3707−3713.
(83) Koster, L. J. A.; Kemerink, M.; Wienk, M. M.; Maturová, K.; Janssen, R. A. J. Quantifying Bimolecular Recombination Losses in

https://doi.org/10.1021/acsapm.1c01856
ACS Appl. Polym. Mater. 2022, 4, 1991−2005

Organic Bulk Heterojunction Solar Cells. *Adv. Mater.* **2011**, *23* (14), 1670−1674.

https://doi.org/10.1021/acsapm.1c01856
ACS Appl. Polym. Mater. 2022, 4, 1991−2005